PIMS

Proceedings of International Mathematical Sciences

VOLUME I
ISSUE 2

VOLUME I ISSUE II December 2019
https://dergipark.org.tr/tr/pub/pims

PROCEEDINGS OF INTERNATIONAL MATHEMATICAL SCIENCES

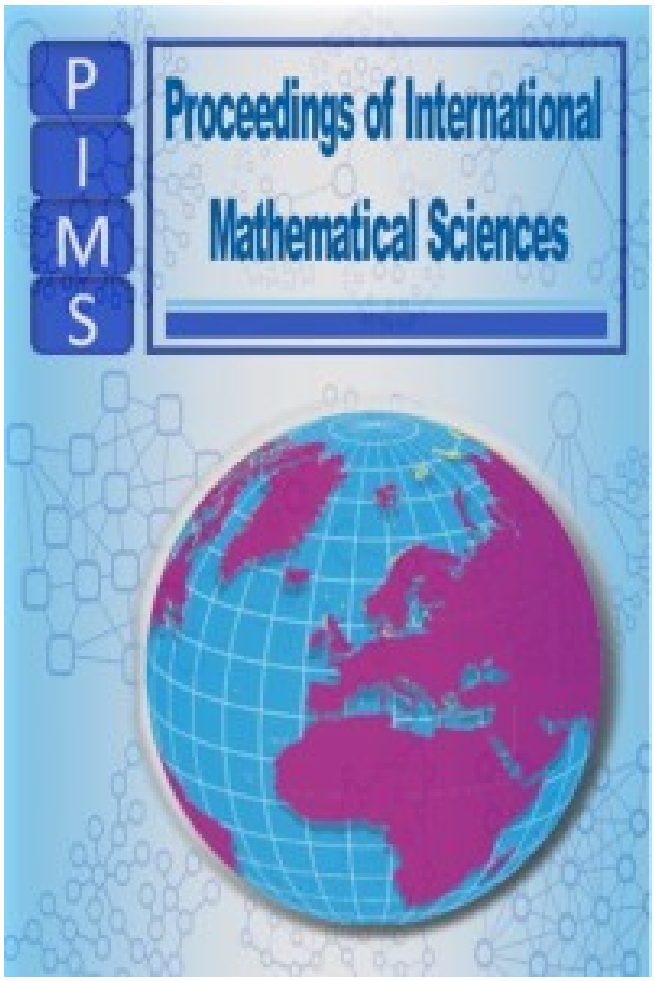

Editor-in-Chief

Hüseyin Çakallı
Maltepe University, Istanbul, Turkey
hcakalli@gmail.com

Managing Editor

Fuat Usta
Düzce University, Düzce, Türkiye
fuatusta@duzce.edu.tr

Editorial Board

Publishing Board

Contents

1 A Block-Based Image Encryption Scheme Using Cellular Automata with Authentication Capability
Saeideh Kabirirad , Ziba Eslami **41-50**

2 Pitchfork Domination and It's Inverse for Corona and Join Operations in Graphs
Mohammed A. Abdlhusein , Manal N. Al-Harere **51-55**

3 Soliton Solutions of Gursey Model with Bichromatic Force
Eren Tosyalı , Fatma Aydogmus **56-59**

4 A Mathematical Model of a Zika Virus Transmission with Impact of Awareness by Media
Puji Andayani **60-68**

5 The Explicit Relation Between the DKP Equation and the Klein-Gordon Equation
Djahida Bouchefra , Badredine Boudjedaa **69-76**

Proceedings of International Mathematical Sciences
URL: https://dergipark.org.tr/tr/pub/pims
Volume I Issue 2 (2019), Pages 41-50.

A BLOCK-BASED IMAGE ENCRYPTION SCHEME USING CELLULAR AUTOMATA WITH AUTHENTICATION CAPABILITY

SAEIDEH KABIRIRAD * AND ZIBA ESLAMI**

*DEPARTMENT OF COMPUTER SCIENCE, BIRJAND UNIVERSITY OF TECHNOLOGY, BIRJAND, IRAN

**(CORRESPONDING AUTHOR) DEPARTMENT OF DATA AND COMPUTER SCIENCE, SHAHID BEHESHTI UNIVERSITY, G.C., TEHRAN, IRAN

Abstract. In this paper, we employ a combination of chaotic maps and Cellular automata(CA) to propose a secure block-based image encryption scheme with authentication capability. The authentication mechanism incorporated into the presented scheme can detect slight tampering in the cipher image before full decryption. We use chaotic maps to produce pseudo-random sequences and apply a CA to diffuse the pixel values efficiently. Many of the existing image encryption schemes fall short of providing parallel processing capability and high sensitivity to changes simultaneously. This study tries to provide both capabilities together. Furthermore, our proposed authentication mechanism, while preventing exploitation in brute-search attacks, can be adjusted to any desired level of security. Finally, theoretical analysis and experimental results together with comparisons with related literature indicate that the proposed scheme has a high robustness against common security attacks.

1. Introduction

One of the most widely used systems in the image encryption is chaos systems. Some of the special features of chaos systems include their dependency to initial conditions and control parameters and their ergodic characteristics. Therefore, their application in cryptography provides high complexity, random-like behavior, diffusion and thus better security. Researchers have proposed different chaos based image encryptions in [1, 2, 3]. Overall, to resist common attacks, these schemes have two phases: confusion and diffusion [4]. In the confusion phase plain image is disturbed that the correlation between two adjacent pixels is extremely low and in the diffusion phase the pixel values are altered so that the influence of individual plain image is spread out over the cipher image as much as possible [5]. Furthermore considering the security analysis such as [6], it can be concluded that the encryption key sequence must also be related to the image pixels, otherwise it will be susceptible

2010 *Mathematics Subject Classification.* Primary: 68P25 ; Secondaries: 94A60 .
Key words and phrases. Image Encryption; Cellular Automata; Chaotic Map; Authentication.

to attacks such as known or chosen plain-text attacks. Also, these methods might not be sufficiently sensitive to plain image.

For more computational efficiency, some researchers use tools such as cellular automata (CA) [7, 8, 9] and linear feedback shift registers [10]. CA are discrete dynamical system formed by a finite array of identical objects called cells. Each cell is endowed with a state which changes at every time-step depending on the states of its adjacent cells at previous time-steps. This feature provides confusion and therefore makes CA attractive in cryptography. Furthermore, they have parallel computation capability as well as high execution speed.
In the CA-based method presented in [11], permutation and diffusion stages are implemented in two separate phases. In permutation phase, pixels of the plain image are shuffled using a pseudo-random keystream generated by intertwining logistic chaotic map. In diffusion phase a two-dimensional CA is applied to achieve diffusion on bit-level. This method does not have complete parallel execution capability, because its permutation phase must be executed in order. The algorithms presented in [7] and [12] used second-order CA. In both papers, the proposed algorithms act like a block-cipher but in a fully parallel mode. Since the blocks are encrypted independently, slight changes in one block has no effect on other blocks. Ping et al. [8] used a second-order, non-affine balanced and reversible CA to increase confusion and diffusion of the encryption algorithm. Also, an irreversible CA is used to produce a pseudo-random key sequence. The diffusion is performed by the local interaction among cells, while the confusion is achieved by the nonlinear rules applied to cells. The method has a good execution speed but cannot be executed in parallel. In [1], an image encryption based on non-uniform cellular automata and hyper chaotic functions is proposed. First, six chaotic sequences using three-dimensional Arnold mapping are generated after frequent iterations. Then random sequences are used to permute the image in rows and columns. In confusion step, a key image created using CA and a hyper-chaotic mapping are used to encrypt the pixels. Reviewing existing literature clarifies most of them cannot provide simultaneously parallel processing capability and high sensitivity to changes [2, 3].
Also, some of image encryption schemes [13] check the integrity of cipher images using an authentication mechanism such that any tampering in the cipher images can be detected.

In this paper, we use the advantages of chaotic maps and CA to present a secure block-based image encryption scheme. This means that we use chaotic maps to produce pseudo-random sequences and apply a CA to diffuse the pixel values with efficiency in a parallel setting. This study tries to provide both capabilities together. Furthermore we augment the authentication mechanism while also preventing exploitation in brute-search attacks and can be adjusted to any desired level of security. Finally, theoretical analysis and experimental results indicate that the proposed scheme has a high robustness against common security attacks.

2. Preliminaries on Cellular Automata

Cellular automata (CA) are dynamic systems consisting of an array of similar units called cells. A CA is defined in the form of $CA = \{\mathcal{C}, \mathcal{S}, \mathcal{N}, \mathcal{F}\}$ where $\mathcal{C}$ is the cell space, $\mathcal{S}$ is the set of discrete states of cells where in the simplest state $\mathcal{S} \in \{0, 1\}$, $\mathcal{N}$ signifies the neighbors of a cell and $\mathcal{F}$ is the transition function,

which includes rules for determining the next state of the cell [14]. Assuming that a_i^T describes the state of cell i in time step T, the local transition function of CA is defined as below:

$$a_i^{T+1} = f(\mathcal{N}_i^T),\ 0 \leq i \leq N-1 \tag{2.1}$$

In the above equation, $\mathcal{N}_i^T$ describes the state of neighbors of cell i in time step T. This formula expresses that the next state of each cell is determined according to a transition function with inputs the current state of itself and its neighbors. States of all cells at time step T form a configuration. In this paper we use a reversible linear memory CA (LMCA). In a LMCA of order t, the next states of the cells depend on t previous configurations which is defined as follows:

$$a_i^{T+1} = f_1(\mathcal{N}_i^T) + f_2(\mathcal{N}_i^{T-1}) + \cdots + f_t(\mathcal{N}_i^{T-t+1}) \tag{2.2}$$

In the above equation, $f_i,\ i = 1, \ldots, t$ are local transition functions in LMCA. If $f_t(\mathcal{N}_i^{T-t+1}) = a_i^{T-t+1}$, then LMCA is reversible through the said transition function and its inverse is another LMCA with the following local transition function:

$$a_i^{T+1} = \sum_{m=0}^{t-2} f_{t-m-1}(\mathcal{N}_i^{T-m}) + a_i^{T-t+1},\ 0 \leq i \leq N-1 \tag{2.3}$$

3. The proposed method

To provide parallel processing capability, we first divide the image into multiple blocks. Then each block is encrypted using an m-order LMCA. A permutation algorithm is performed in block level to eliminate the relation between consecutive blocks. This approach increases the execution speed in comparison to pixel or bit permutation. Finally, second pass of the m-order LMCA with new transition rules is performed. To increase the complexity of the method, LMCA rules are determined by a pseudo-random sequence. We generate the pseudo-random sequence using logistic chaotic map defined according to the following formula:

$$x_i = \alpha x_{i-1}\ (1 - x_{i-1}),\ x_i \in [0, 1] \tag{3.1}$$

where α is the logistic map parameter. The output sequence is chaotic when $\alpha \in [3.57, 4]$.

Since each block is encrypted independently, the values of its pixels have no effect on other encrypted blocks. To create such effect, the hashed value of an interleaved image is calculated and is incorporated in the encryption process. This value is defined such that it is used in authentication as well as encryption.

In the following, image encryption and decryption algorithms are described in detail. Also, graphical representation of the encryption algorithm is depicted in Figure 1.

3.1. **Encryption algorithm.** We assume that plain image P is an image of size $M \times N$. Suppose that number of blocks is nb and size of each block is $m \times n$. The encryption process includes the following steps:

(1) Consider the pixels of image P in the form of array $P = [P_0, P_{nb}, P_{2nb}, \ldots, P_1, P_{nb+1}, \ldots, P_{nb-1}, \ldots, P_{MN}]$ where the image pixels are numbered from top to bottom and left to right. Then, starting from the beginning of the array, we put each mn pixels into a separate block of size $m \times n$. With this simple reorganization, adjacent pixels will probably not be in a block. Assume that blocks are represented by $B_1, B_2, \ldots, B_{nb}$.

FIGURE 1. Diagram of the encryption procedure

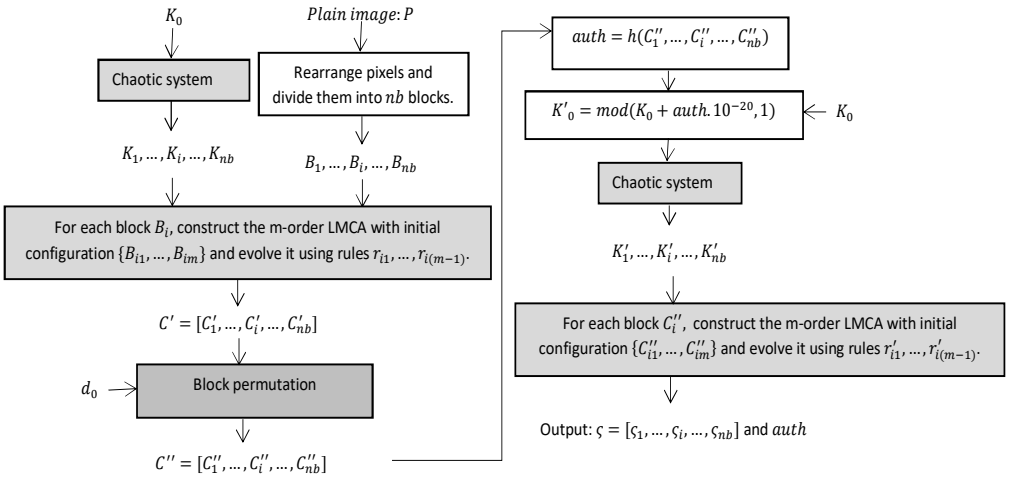

(2) Consider values K_0 and d_0 as the encryption keys. K_0 is the initial value for generating the LMCA rules and d_0 is the initial value for generating the block permutation sequence.
(3) Repeat logistic chaotic map, starting from initial value K_0 for producing nb numbers $[K_1, K_2, \dots, K_{nb}]$. Each of these numbers will be used for producing the LMCA rules in a block.
(4) Then for each block $B_i, i = 1, 2, \dots, n$, perform the following:
   (a) Construct the m-order LMCA with initial configuration $C_i^0 = \{B_{i1}, B_{i2}, \dots, B_{im}\}$, where B_{ij} is the j-th row in i-th block.
   (b) Produce a set of rules $R_i = \{r_{i1}, r_{i2}, \dots, r_{i(m-1)}\}$ using initial value K_i such that: $[r_{i1}, r_{i2}, \dots, r_{i(m-1)}] = f(K_i)$, where f is a function that assigns a random bit sequence to the LMCA rules.
   (c) Evolve the LMCA at least m times starting from the initial configuration to obtain the final configuration $C_i^{'} = \{C_{i1}^{'}, C_{i2}^{'}, \dots, C_{im}^{'}\}$.
(5) In this step, a permutation is conducted on the image blocks using key d_0 to obtain image $C^{''}$.
   (a) First, produce the initial value through $d_0^{'} = mod\ (d_0 + (C_1^{'} \oplus \dots \oplus C_{nb}^{'})10^{-20}, 1)$, where $\oplus$ is XOR operation and $mod(x, 1)$ is the decimal part of x.
   (b) Generate the sequence $d_1, d_2, \dots, d_{nb}$ using the logistic chaotic map with initial value d_0.
   (c) Compute the permutation sequence y such that: $y_i = [d_i \times nb] + 1$
   (d) The set $y_1, y_2, \dots, y_{nb}$ is sorted increasingly and a new set $y_1^{'}, y_2^{'}, \dots, y_{nb}^{'}$ is obtained.
   (e) Determine the new position of each block according to sequence $y^{'}$; to do so, find the position of values $y_1^{'}, y_2^{'}, \dots, y_{nb}^{'}$ in $y_1, y_2, \dots, y_{nb}$ and

the position set $S = \{pos_1, pos_2, \ldots, pos_{nb}\}$ is formed, where $y_i^{'}$ is the value of y_{pos_i}.

(6) Calculate hashed value $auth$ using the permutated image $C^{''}$ as: $auth = h(C_1^{''}, C_2^{''}, \ldots, C_{nb}^{''})$, where $h : Z_{256}^{*} \to Z_{256}^{l}$ is a collision resistant hash function. The value of l is optional and depends on the desired authentication strength.

(7) Produce new initial value $K_0^{'}$ for generating the rules of the second pass of the LMCA as:
$K_0^{'} = mod(K_0 + 10^{-20} auth, 1)$, where $mod(x, 1)$ is the decimal part of x.

(8) Produce the new sequence $K_1^{'}, K_2^{'}, \ldots, K_{nb}^{'}$ and local rules $R_i = \{r_{i1}^{'}, r_{i2}^{'}, \ldots, r_{i(m-1)}^{'}\}$ just like the Steps 3 and 4.

(9) For each block, execute the LMCA at least m times with initial configuration $C_i^{''(0)} = (C_{i1}^{''}, C_{i2}^{''}, \ldots, C_{im}^{''})$ and local rules $r_{i1}^{'}, r_{i2}^{'}, \ldots, r_{i(m-1)}^{'}$; In the end, the final configuration $\varsigma_i = \{\varsigma_{i1}, \varsigma_{i2}, \ldots, \varsigma_{i(m)}\}$ will be obtained.

The final cipher image is obtained as $CI = \{\varsigma_1, \varsigma_2, \ldots, \varsigma_{nb}, auth\}$. Here, $auth$ will be used for producing the key sequence as well as in errors detection.

3.2. **Decryption algorithm.** To decrypt cipher image $CI = \{\varsigma_1, \varsigma_2, \ldots, \varsigma_{nb}, auth\}$ with the key (K_0, d_0), the steps of the encryption algorithm must be followed in reverse. For checking the validity of the cipher image, we must calculate value: $H = h(C_1^{''}, C_2^{''}, \ldots, C_{nb}^{''})$ after evolving the reverse of LMCA in the first pass. If $H = auth$, the image is authenticated.

4. SECURITY ANALYSIS AND EXPERIMENTAL RESULTS

In this section, the security analysis of the proposed scheme and its experimental results are provided. We implemented the proposed algorithm and evaluated this with various images. For example, we run algorithm with plain images of Figure 2(a),(b) of size 512×512 and obtained corresponding cipher images of Figure 2(c),(d).

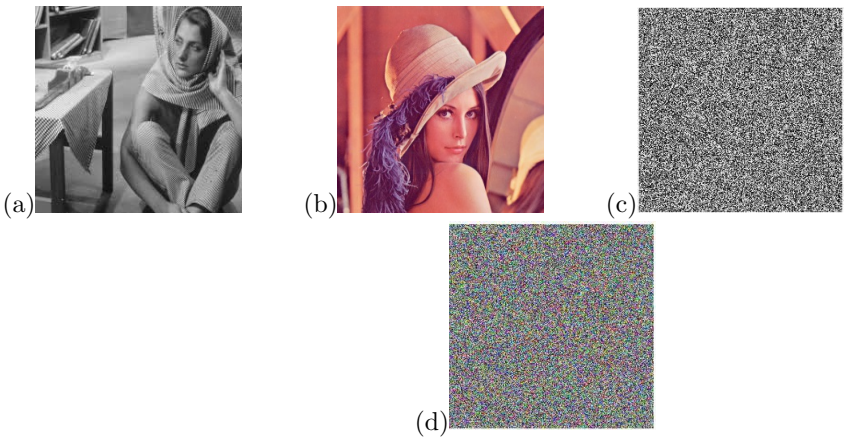

FIGURE 2. (a),(b) Plain images "Barbara" and "Lena"; (c),(d) and corresponding encrypted images.

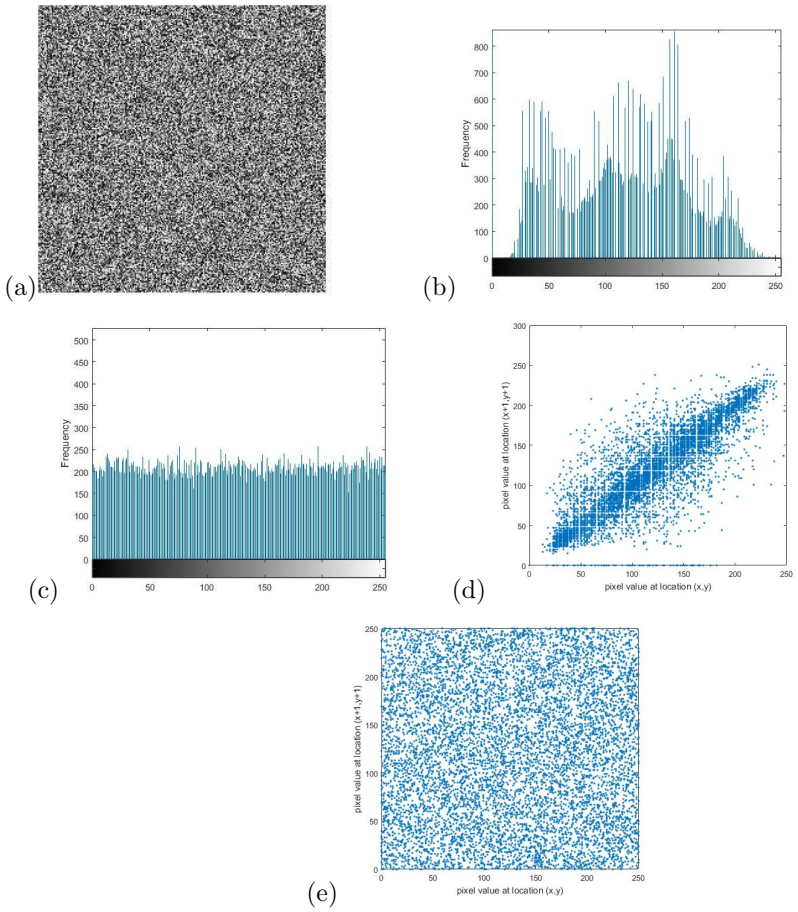

FIGURE 3. (a) Decrypted image of Barbara by a slightly changed key; (b),(c) Histograms of the plain image "Barbara" and the corresponding cipher image; (d),(e) Plots of the intensity values of adjacent pixels in diagonal direction.

(1) **Chosen plain-image attacks.** In this attack, the attacker has a temporary access to the encryption system and chooses a number of plain-images and obtains their corresponding cipher-images. Then he tries to break the cryptosystem. Without knowing the encryption key, decryption is impossible. Because of Steps 5 and 7 in the encryption algorithm, values of pixels also affect the key sequence; So this sequence will be different for various images. As a result, it is impossible to use a key sequence resulted from a chosen plain-image on a different or even roughly similar image. Therefore this method is resistant against chosen plain-image or known plain-image attacks.

(2) **Key space and sensitivity analysis.** For an encryption scheme to be secure, it must has a sufficiently large key space. In the encryption algorithm, length of key (K_0, d_0) is at least 150 bits, so the key space is at least

2^{150}. As a result, this method is also resistant against brute-force attacks. Experimental results show that this method is sensitive to the key. For example, we have decrypted image of Figure 2(c) with slightly different key value and have obtained image of Figure 3(a). Comparing the recovered image with original one reveals that their pixels are totally different.

(3) **Histogram analysis.** Histogram analysis determines distribution of image pixels. Histogram of the cipher image must be almost uniform and have a significant difference with the histogram of the plain image to prevent the attacker from extracting any meaningful information. Figure 3(b),(c) shows the histograms of the plain and corresponding cipher images.

(4) **Correlation analysis of adjacent pixels.** Pixels of a plain image often have significant dependency, but dependency of cipher image pixels must be negligible. To test the correlation of adjacent pixels in an image, we randomly choose pairs of adjacent pixels and use the following formula to calculate the correlation coefficient in vertical, horizontal and diagonal directions.

$$\sigma_{uv} = \frac{\sum_{i=1}^{N}(u_i - mean(u))(v_i - mean(v))}{\sum_{i=1}^{N}((u_i - mean(u))^2)^{1/2}\sum_{i=1}^{N}((v_i - mean(v))^2)^{1/2}} \tag{4.1}$$

In the above equation, u and v are the arrays of N adjacent pixels. The correlation coefficients of adjacent pixels in some plain and cipher images are summarized in Table 1. Also Figure 3(c),(d) shows plots of the intensity values of 10000 couples of horizontally adjacent pixels in plain image "Barbara" and the corresponding cipher image.

(5) **Differential attack.** In this attack, the attacker makes a slight change in the plain image and compares its cipher image with original one to find a significant relationship. The presented algorithm is robust against this attack, because the LMCA distributes any change in its input on its final output, so a small change in a block of plain image affects the entire block. Furthermore, after the first round of execution of the LMCA, a hashed value of the entire resulting pixels is calculated and is used in the second round. Note that, one of the main features of a hash function is that even a slight change in its inputs makes substantial changes in its output. Thus any small change in a block of the plain image triggers extensive changes in the hashed value, the key sequence and consequently cipher image.
Also, we assess robustness of the proposed scheme against the attack with the use of two measures: NPCR (Number of Pixels Change Rate) and UACI (Unified Averaged Changed Intensity) which are calculated with the following formulas.

$$NPCR = \frac{\sum_{i=1}^{M}\sum_{j=1}^{N} d(i,j)}{M \times N} \times 100\%$$

$$UACI = \frac{1}{M \times N}\sum_{i=1}^{M}\sum_{j=1}^{N}\frac{|p(i,j) - q(i,j)|}{255} \times 100\%$$

In the above equations, p and q are the sets of pixels of the original and the changed images, respectively. If $p(i,j) = q(i,j)$ then $D(i,j) = 0$ otherwise $D(i,j) = 1$.

We have encrypted several images using the proposed method and calculated the values of NPCR and UACI. A summary of the obtained results are presented in Table 1. The value of NPCR is close to 100% and the value of UACI is close to 33.5%, which indicate the high sensitivity of the proposed scheme to the plain image.

(6) **Information entropy analysis.** The information entropy is the most significant measure of unpredictability of information. The information entropy $H(I)$ of an image I can be calculated by the following formula:

$$H(I) = -\sum_{i=1}^{l} P(I_i) log_2 P(I_i) \tag{4.2}$$

where l is the total number of pixels in I and $p(I_i)$ represents the probability of occurrence of value I_i. For a random image emitting 256 values with the same probability, $H(I)$ reaches the maximum value 8. The entropy values for some ciphers are summarized in the last column of Table 1. It can be observed that they are close to a random source.

TABLE 1. The correlation coefficients, the average NPCR and UACI and entropy of the proposed scheme.

Image	Horizontal		Vertical		Diagonal		Average	Average	Entropy
	Plain	Cipher	Plain	Cipher	Plain	Cipher	NPCR	UACI	
Barbara	0.9132	0.0091	0.9360	-0.0512	0.9720	0.0990	99.606	33.461	7.9992
Lena	0.895	0.0120	0.9041	0.0074	0.8912	-0.0814	99.611	33.518	7.9993
Cameraman	0.9597	0.0355	0.9381	-0.0019	0.9325	0.0189	99.581	33.521	7.9993
Peppers	0.9655	-0.0027	0.9761	0.0712	0.9428	0.0089	99.594	33.361	7.9994

4.1. **Validity of the authentication algorithm.** The presented scheme has an authentication phase in the decryption algorithm. The authentication is performed on image obtained from evolving the inverse of LMCA in the first round. The value of H is calculated the same as stage 6 of the encryption algorithm and is compared with the value of $auth$. If these values are not equal, the cipher image has errors. The value of $auth$ is produced using the intermediate values of the encryption process and is calculated by a collision-resistant hash function, so it will not reveal any information about the plain image. Also, considering the use of hash function to produce $auth$ and sufficient complexity of the LMCA, the chance of manipulating the cipher image such that the values of H and $auth$ would be equal is very negligible. Therefore, any tampering on the cipher image can be detected.

5. COMPARISON

In the following, we compare the proposed method with the methods presented in [1, 7, 8, 11] in terms of cipher image sensitivity, parallel execution capability, block or string nature of algorithm and etc.

Algorithms in [13, 11] use a stream-cipher scheme in the permutation phase and block-cipher scheme in the diffusion phase; while other assessed algorithms are totally block-based. Therefore they cannot provide full parallel processing capability, since it takes a lot of time to execute the sort algorithm in the permutation phase.

Scheme [8] cannot be executed in parallel efficiently.
In terms of sensitivity to the plain image, algorithms [11, 7] cannot be considered sufficiently sensitive, because in these algorithms changing a pixel does not affect the previous encrypted pixels or the entirety of pixels. In the proposed method and methods [1, 8], the encryption key sequence is affected by pixels, so any slight change in the plain image affects all pixels in the cipher image.
The proposed scheme and [13] can check integrity by adding extra bits in the cipher image. In [13] a fixed number of authentication bits (8 bits per block) is used, while in our scheme this parameter is tunable to any arbitrary value.
In all mentioned methods except the method of [8], the confusion and diffusion stages are applied in two separate phases. None of the compared schemes [8, 7, 1, 13, 11] can ensure sensitivity of the entire cipher-image to the plain-image and at the same time provide parallel execution capability. But the proposed scheme could be executed in parallel while also providing high sensitivity to the plain image. A summary of the results of the comparison is presented in table 2.

Table 2. Comparisons between the proposed scheme and similar schemes

	Our scheme	[13]	[7]	[1]	[8]	[11]
Block-based	✓	✓	✓	✗	✓	✓
Parallel computing	✓	✗	✓	✗	✗	✗
High sensitivity	✓	✗	✗	✓	✓	✗
Authenticated	✓	✓	✗	✗	✗	✗
Simultaneous confusion and diffusion	✗	✗	✓	✗	✓	✗

6. CONCLUSION

This paper proposes an image encryption scheme based on chaotic maps and linear memory cellular automata. In this method, the encryption and decryption of image is block-based. To determine the integrity of the cipher image, an authentication mechanism is provided which can detect manipulation in the image. A prominent point of the proposed method is the combination of parallel execution capability with high sensitivity of cipher image to slight changes in the plain image. Security analysis and experimental results demonstrate that the presented scheme fulfills all the desired properties of a secure cryptosystem including large key space, statistical attacks, differential attack and chosen-plaintext attack.

References

[1] A.Y. Niyat, M. H. Moattar, and M. N. Torshiz, Color image encryption based on hybrid hyper-chaotic system and cellular automata, Optics and Lasers in Engineering **90**, 225-237 (2017).
[2] A. Souyah, and K. M. Faraoun, Fast and efficient randomized encryption scheme for digital images based on quadtree decomposition and reversible memory cellular automata, Nonlinear Dynamics **84**,715-732 (2016).
[3] L. Xu, Z. Li, J. Li, and W. Hua, A novel bit-level image encryption algorithm based on chaotic maps, Optics and Lasers in Engineering **78**, 17-25 (2016).
[4] C. E. Shannon, Communication theory of secrecy systems, Bell system technical journal **28**, 656-715 (1949).
[5] G. Alvarez, and S. Li, Some basic cryptographic requirements for chaos-based cryptosystems, International journal of bifurcation and chaos **16(22)**, 2129-2151 (2006).

[6] H. Liu, and Y. Liu, Cryptanalyzing an image encryption scheme based on hybrid chaotic system and cyclic elliptic curve, Optics & Laser Technology **56**, 15-19 (2014).
[7] K. M. Faraoun, A parallel block-based encryption schema for digital images using reversible cellular automata, Engineering Science and Technology, an International Journal **17**, 85-94 (2014).
[8] P. Ping, F. Xu, and Z. J. Wang, Image encryption based on non-affine and balanced cellular automata, Signal Processing **105**, 419-429 (2014).
[9] B. Jeyaram and R. Raghavan, New cellular automata-based image cryptosystem and a novel non-parametric pixel randomness test, Security and Communication Networks **9**, 3365-3377 (2016).
[10] D. Dey, D. Giri, B. Jana, T. Maitra and R.N. Mohapatra, Linear-feedback shift register-based multi-ant cellular automation and chaotic map-based image encryption, Security and Privacy **1(6)**, 1-11 (2018).
[11] X. Wang and D. Luan, A novel image encryption algorithm using chaos and reversible cellular automata, Communications in Nonlinear Science and Numerical Simulation **18(11)**, 3075-3085 (2013).
[12] K. M. Faraoun, Fast encryption of RGB color digital images using a tweakable cellular automaton based schema, Optics & Laser Technology, **64**, 145-155 (2014).
[13] A.S. Rajput and M.A. Sharma, Novel Image Encryption and Authentication Scheme Using Chaotic Maps, In Advances in Intelligent Informatics, Springer, Cham, 277-286 (2015).
[14] S. Wolfram, Cellular automata and complexity, collected papers. CRC Press (2018).

S. Kabirirad,
Birjand University of Technology, Birjand, Iran, Phone: +985632391144
Email address: s_kabirirad@sbu.ac.ir

Z. eslami,
Shahid Beheshti University, Tehran, Iran, Phone: +982129903007
Email address: z_eslami@sbu.ac.ir

Proceedings of International Mathematical Sciences
URL: https://dergipark.org.tr/tr/pub/pims
Volume I Issue 2 (2019), Pages 51-55.

PITCHFORK DOMINATION AND IT'S INVERSE FOR CORONA AND JOIN OPERATIONS IN GRAPHS

MOHAMMED A. ABDLHUSEIN*, AND MANAL N. AL-HARERE**

*DEPARTMENT OF MATHEMATICS, COLLEGE OF EDUCATION FOR PURE SCIENCES (IBN AL-HAITHAM), BAGHDAD UNIVERSITY, BAGHDAD, IRAQ, PHONE: 009647808271658

**DEPARTMENT OF APPLIED SCIENCES, UNIVERSITY OF TECHNOLOGY, BAGHDAD, IRAQ, PHONE: 009647703913468

Abstract. Let G be a finite simple and undirected graph without isolated vertices. A subset D of V is a pitchfork dominating set if every vertex $v \in D$ dominates at least j and at most k vertices of $V - D$, where j and k are non-negative integers .The domination number of G, denoted by $\gamma_{pf}(G)$ is a minimum cardinality over all pitchfork dominating sets in G. A subset D^{-1} of $V - D$ is an inverse pitchfork dominating set if D^{-1} is a pitchfork dominating set. The inverse domination number of G, denoted by $\gamma_{pf}^{-1}(G)$ is a minimum cardinality over all inverse pitchfork dominating sets in G. In this paper, the pitchfork domination and the inverse pitchfork domination are determined when $j = 1$ and $k = 2$ for some graphs that obtained from graph operations corona and join.

1. Introduction

Let $G = (V, E)$ be a graph without isolated vertices with vertex set V of order n and edge set E of size m. The complement $\bar{G}$ of a simple graph G with vertex set $V(G)$ is the graph in which two vertices are adjacent if and only if they are not adjacent in G. The join $G_1 + G_2$ between two graphs G_1 and G_2 is a graph contains all edges and vertices of both graphs and every vertex of G_1 joined by edges with all vertices of G_2. The corona $G_1 \odot G_2$ between two graphs G_1 and G_2 is a graph has one copy of G_1 and $|V(G_1)|$ copies of G_2 such that the i^{th} vertex of G_1 joined by edges with all vertices of the i^{th} copy of G_2. For graph theoretic terminology we refer to [6] and [10]. For a detailed survey of domination one can see [7] and [8]. A set $D \subseteq V$ is a dominating set if every vertex in $V - D$ is adjacent to a vertex in D. If no proper subset of D is a dominating set then D is said to be minimal . The domination number $\gamma(G)$ is the minimum cardinality of a dominating set D of G. There are many papers deals with different types of domination, such as [3], [4], [5], [9].

2010 *Mathematics Subject Classification.* 05C69.
Key words and phrases. pitchfork domination; inverse pitchfork domination; corona operation.

Here, a new model of domination in graphs called the pitchfork domination and it's inverse, which were studied in [1, 2], are applied on some graphs formed by using two types of operations.

Theorem 1.1. [2] *The cycle graph C_n with $n \geq 3$ has an inverse pitchfork domination such that: $\gamma_{pf}^{-1}(C_n) = \gamma_{pf}(C_n) = \lceil \frac{n}{3} \rceil$.*

Proposition 1.2. [1] *Let $G = K_n$ the complete graph with $n \geq 3$, then $\gamma_{pf}(K_n) = n - 2$.*

Proposition 1.3. [2] *The complete graph K_n has an inverse pitchfork domination if and only if $n = 3, 4$ and $\gamma_{pf}^{-1}(K_n) = n - 2$.*

Theorem 1.4. [1] *Let G be the complete bipartite graph, then:*

$$\gamma_{pf}(K_{n,m}) = \begin{cases} m, & \text{if } n = 2 \wedge m < 3 \quad or \quad n = 1 \wedge m > 2 \\ m - 1, & \text{if } n = 2, m \geq 3 \\ n + m - 4, & \text{if } n, m > 2. \end{cases}$$

Theorem 1.5. [2] *The complete bipartite graph $K_{n,m}$ has an inverse pitchfork domination if and only if $K_{n,m} \equiv K_{1,2}, K_{2,2}, K_{2,3}, K_{2,4}, K_{3,3}, K_{3,4}$ or $K_{4,4}$ such that:*

$$\gamma_{pf}^{-1}(K_{n,m}) = \begin{cases} 2 & for\ K_{1,2} \\ n + m - 4 & if\ n,\ m\ =\ 2,\ 3,\ 4 \end{cases}$$

Proposition 1.6. [1] *For any graph G having a pitchfork domination set, if G has a support vertex, that is adjacent to more than two pendents then all it's pendents belong to the pitchfork dominating set.*

Note 1.7. [2] *If $\gamma_{pf}(G) > \frac{n}{2}$ then G has no inverse pitchfork domination.*

Proposition 1.8. [2] *Let G be a graph which has a support vertex adjacent to more than two pendent vertices, then G has no inverse pitchfork domination.*

2. The Main Results

The pitchfork domination and the inverse pitchfork domination are studied here for some graphs constructed by corona or join operations.

Theorem 2.1. *If G is a graph of order n, then:*
1- $\gamma_{pf}(G \odot K_2) = \gamma_{pf}(\overline{G} \odot K_2) = \gamma_{pf}(G \odot \overline{K}_2) = \gamma_{pf}(\overline{G} \odot \overline{K}_2) = n.$
2- $\gamma_{pf}(G + K_2) = \gamma_{pf}(\overline{G} + K_2) = \gamma_{pf}(G + \overline{K}_2) = \gamma_{pf}(\overline{G} + \overline{K}_2) = n.$
3- $\gamma_{pf}(G \odot \overline{K}_1) = \gamma_{pf}(\overline{G} \odot \overline{K}_1) = n.$

Proof. Let $D \subseteq V$. 1 and 2: Since every $v \in G$ is adjacent to two vertices of K_2 or $\overline{K}_2$, then $v \in D$. Therefore, every $v \in D$ dominates exactly two vertices. Thus, D is $\gamma_{pf}-$set and $D = V(G)$ with order n . Others cases are proved by the same way. 3: Since every support vertex or it's leaf belongs to D, then $D = V(G)$ is a $\gamma_{pf}-$set. □

Theorem 2.2. *If G is a graph of order n, then:*
1- $\gamma_{pf}^{-1}(G \odot K_2) = \gamma_{pf}^{-1}(\overline{G} \odot K_2) = n.$
2- $\gamma_{pf}^{-1}(G \odot \overline{K}_2) = \gamma_{pf}^{-1}(\overline{G} \odot \overline{K}_2) = 2n.$
3- $\gamma_{pf}^{-1}(G \odot \overline{K}_1) = \gamma_{pf}^{-1}(\overline{G} \odot \overline{K}_1) = n.$

Proof. Let $D \subseteq V$. 1- There are n cycles of order three and $\gamma_{pf}^{-1}(C_3) = 1$ according to Theorem 1.1. The result is obtained.
2- Every vertex of G or $\overline{G}$ is a support vertex and is adjacent to two (non-adjacent) vertices of $\overline{K_2}$. So that, D contains all vertices of G or $\overline{G}$ according to Theorem 2.1 part 1. Therefore, $D^{-1} = V - D$ which has all vertices of the copies of $\overline{K}_2$. Hence, $\gamma_{pf}^{-1} = 2n$.
3- Similar to proof in Theorem 2.1 case 3. □

Theorem 2.3. *$G + K_2$, $\overline{G} + K_2$, $G + \overline{K}_2$ and $\overline{G} + \overline{K}_2$, have an inverse pitchfork domination if and only if $n \leq 2$ such that:*
1- $\gamma_{pf}^{-1}(G + K_2) = \gamma_{pf}^{-1}(\overline{G} + K_2) = n$.
2- $\gamma_{pf}^{-1}(G + \overline{K}_2) = \gamma_{pf}^{-1}(\overline{G} + \overline{K}_2) = 2$.

Proof. 1- If $n = 1$ then $G + K_2 = \overline{G} + K_2 = C_3$ which has $\gamma_{pf}^{-1}(C_3) = 1$ by Theorem 1.1. If $n = 2$ then $D = V(G)$ by Theorem 2.1. So, $D^{-1} = V(K_2)$ which is a $\gamma_{pf}^{-1}-$set of order 2.
2- Since every $v \in G$ or $\overline{G}$ is adjacent to two vertices of $\overline{K}_2$ and $v \in D$ from Theorem 2.1, then we have $D^{-1} = V(\overline{K}_2)$. Hence, D^{-1} dominates all vertices of the graph and it is an inverse pitchfork dominating set. Every $w \in D^{-1}$ dominates exactly two vertices of G or $\overline{G}$. Therefore, D^{-1} is a $\gamma_{pf}^{-1}-$set of order 2. Now, If $n \geq 3$ then the graph has no inverse pitchfork domination by Note 1.7 since $\gamma_{pf} > \frac{n+2}{2}$. □

Theorem 2.4. *For K_m with $m \geq 3$ and G of order n, we have:*
1- $\gamma_{pf}(G \odot K_m) = \gamma_{pf}(\overline{G} \odot K_m) = n(m-1)$.
2- $\gamma_{pf}(G \odot \overline{K}_m) = \gamma_{pf}(\overline{G} \odot \overline{K}_m) = nm$.

Proof. 1- $\gamma_{pf}(K_m) = m - 2$ by Proposition 1.2 then there are two vertices in every copy of K_m which are not in D. But all the vertices from every copy of K_m which are adjacent to one vertex of G. Then we must add to D one vertex from every copy of K_m. Hence, D is a pitchfork dominating set that contains $m - 1$ vertices from every copy of K_m. Since, every vertex of D dominates exactly two vertices, therefore D is a $\gamma_{pf}-$set with order $n(m-1)$.
2- Since every vertex of G becomes a support vertex and it is adjacent to $m \geq 3$ leaves of $\overline{K}_m$, then by Proposition 1.6, D consists of only the end vertices which are all vertices of n copies of K_m. Hence, $\gamma_{pf}(G \odot \overline{K}_m) = nm$. □

Theorem 2.5. *For K_m with $m \geq 3$ and G of order n, then:*
1. $G \odot K_m$ and $\overline{G} \odot K_m$ has an inverse pitchfork domination if and only if $m = 3, 4$ such that $\gamma_{pf}^{-1}(G \odot K_m) = \gamma_{pf}^{-1}(\overline{G} \odot K_m) = n(m-1)$.
2. $G \odot \overline{K}_m$ and $\overline{G} \odot \overline{K}_m$ has no inverse pitchfork domination.

Proof. 1-K_{m+1} has an inverse pitchfork domination if and only if $m + 1 = 3, 4$ where $\gamma_{pf}^{-1}(K_{m+1}) = m-1$ according to Proposition 1.3. Therefore, $\gamma_{pf}^{-1}(G \odot K_m) = \gamma_{pf}^{-1}(\overline{G} \odot K_m) = n(m-1)$.
2- Since D contains all vertices of the copies of $\overline{K}_m$ by Theorem 2.4. And for all $v \in G$ or $\overline{G}$, then v is a support vertex that joins with more than two pendents. Then $v \notin D^{-1}$ and there is no $\gamma_{pf}^{-1}-$set according to Proposition 1.8. □

Theorem 2.6. *For any graph G of order n and complete graph K_m with $m \geq 3$, we have:*

1. $\gamma_{pf}(G + K_m) = \gamma_{pf}(\overline{G} + K_m) = |V(G)| + \gamma_{pf}(K_m) = n + m - 2$.
2. $G + K_m$ *and* $\overline{G} + K_m$ *has an inverse pitchfork domination if and only if* $n = 1$ *and* $m = 3$ *such that* $\gamma_{pf}^{-1}(G + K_m) = \gamma_{pf}^{-1}(\overline{G} + K_m) = 2$.

Proof. 1- Since $\gamma_{pf}(K_m) = m - 2$ by Proposition 1.2 and since every vertex in G is adjacent with all vertices of K_m, then all vertices of G must belong to the dominating set D. Hence $\gamma_{pf}(G + K_m) = n + m - 2$.
2- It is clear from Proposition1.3. □

Observation 2.7. *Let* G *be a disconnected graph with* $H_1, H_2, \cdots, H_n$ *components, then:*
1- $\gamma_{pf}(G) = \sum_{i=1}^{n} \gamma_{pf}(H_i)$.
2- $\gamma_{pf}^{-1}(G) = \sum_{i=1}^{n} \gamma_{pf}^{-1}(H_i)$.

Theorem 2.8. *For a connected graph* G_1 *of order* $n \geq 2$ *and a null graph* G_2 *of order* $m \geq 2$*, we have:*

$$n + m - 3 \leq \gamma_{pf}(G_1 + G_2) \leq n + m - 2$$

Proof. Let $v_1, v_2 \in V - D$ where $v_1 \in G_1$ and $v_2 \in G_2$. Then any vertex of G_1 which is adjacent to v_1 will dominates v_1 and v_2. Any vertex of G_1 which is not adjacent to v_1 will dominates only v_2. While all vertices of G_2 unless v_2 will dominates only v_1. Therefore, $V - D$ can not take another vertex of G_2. But $V - D$ can contain another vertex from G_1 say u (by condition: G_1 is not a complete graph and there is no vertex in G_1 adjacent with both v_1 and u). Hence $\gamma_{pf}(G_1+G_2) = n+m-3$ when the condition hold. But if the condition doesn't hold, then $\gamma_{pf}(G_1+G_2) = n+m-2$. Therefore, in general $n + m - 3 \leq \gamma_{pf}(G_1 + G_2) \leq n + m - 2$. □

Theorem 2.9. *For any two connected graphs* G_1 *of order* $n \geq 2$ *with* $\gamma_{pf}(G_1)$ *and* G_2 *of order* $m \geq 2$ *with* $\gamma_{pf}(G_2)$*, then:*
1. $\gamma_{pf}(G_1 + G_2) \geq \gamma_{pf}(G_1) + \gamma_{pf}(G_2)$ *and* $\gamma_{pf}(G_1 + G_2) = n + m - 2$.
2. $G_1 + G_2$ *has an inverse pitchfork domination if and only if* $n = m = 2$ *such that* $\gamma_{pf}^{-1}(G_1 + G_2) = n + m - 2$.

Proof. 1- Let $V - D$ consists of two vertices one vertex from G_1 (say v_1) and one from G_2 (say v_2). Since G_1 is a connected graph then for any vertex $u_1 \in G_1$ which is adjacent to v_1, then u_1 dominates v_1 and v_2. Also, since G_2 is a connected graph then for any vertex $u_2 \in G_2$ which is adjacent to v_2, it will dominate v_1 and v_2. The other vertices of G_1 dominate only v_2 and the other vertices of G_2 dominate only v_1. Therefor, all vertices except v_1 and v_2 belong to D which is a $\gamma_{pf}-$set.
2- The proof is clear when $n = m = 2$. If $n + m \geq 5$ then there is no inverse pitchfork domination according to Note 1.7 since $\gamma_{pf}(G_1 + G_2) > \frac{n+m}{2}$. □

Theorem 2.10. *Let* G_1 *and* G_2 *be two null graphs of order* n *and* m *respectively, then:*
1- $\gamma_{pf}(G_1 + G_2) = \gamma_{pf}(K_{n,m})$.
2- $G_1 + G_2$ *has an inverse pitchfork domination if and only if* $n = 1$ *and* $m = 2$ *or* n, $m = 2, 3, 4$ *such that* $\gamma_{pf}^{-1}(G_1 + G_2) = \gamma_{pf}^{-1}(K_{n,m})$.

Proof. Since the bipartite graph formed by joining any two null graphs, then the pitchfork domination and it's inverse given according to Theorem 1.4 and Theorem 1.5. □

Theorem 2.11. *For any two graphs G_1 and G_2, of order n and m respectively $(n, m > 2)$, then:*

$$n + m - 4 \leq \gamma_{pf}(G_1 + G_2) \leq n + m - 2$$

Proof. To prove the lower bound, suppose that G_1 and G_2 are two null graphs having as few edges as possible. Then $\gamma_{pf}(G_1 + G_2) = \gamma_{pf}(K_{n,m}) = n + m - 4$ by Theorem 1.4 and Theorem 2.10. Also, to prove the upper bound, suppose that G_1 and G_2 are two complete graphs. Then $\gamma_{pf}(G_1 + G_2) = \gamma_{pf}(K_{n+m}) = n + m - 2$ by Proposition 1.2. □

3. Conclusion

The pitchfork domination and the inverse pitchfork domination are determined when $j = 1$ and $k = 2$ for some graphs that obtained from two types of operations: corona operation and join operation.

Acknowledgments. We thank Maltepe University for the good organization of the Third International Conference of Mathematical Sciences (ICMS 2019).

References

[1] M. A. Abdlhusein and M. N. Al-harere, *Pitchfork Domination in Graphs*, (2019) reprint.
[2] M. A. Abdlhusein and M. N. Al-harere, *Inverse Pitchfork Domination in Graphs*, (2019) reprint.
[3] M. N. Al-harere and A. T. Breesam, *Further Results on Bi-domination in Graphs*, AIP Conference Proceedings **2096** (2019) 020013-020013-9p.
[4] M. N. Al-harere and P. A. Khuda Bakhash, *Tadpole Domination in Graphs*, *Baghdad Science Journal* **15** (2018) 466-471.
[5] M. Chellali, T. W. Haynes, S. T. Hedetniemi, and A. M. Rae, *[1,2]-Set in graphs*, Discrete Applied Mathematic, **161** (2013) 2885- 2893.
[6] F. Harary, *Graph Theory*, Addison-Wesley, Reading Mass, (1969).
[7] T. W. Haynes, S. T. Hedetniemi and P.J. Slater, *Domination in Graphs -Advanced Topics*, Marcel Dekker Inc., (1998).
[8] S.T. Hedetneimi and R. Laskar, *Topics in domination in graphs*, Discrete Math. **86** (1990).
[9] A. A. Omran and Y. Rajihy, *Some Properties of Frame Domination in Graphs*, Journal of Engineering and Applied Sciences, **12** (2017) 8882-8885.
[10] Ore O. *Theory of Graphs*, American Mathematical Society, Provedence, R.I. (1962).

Mohammed A. Abdlhusein,
Department of Mathematics, College of Education for Pure Sciences (Ibn Al-Haitham), Baghdad University, Baghdad, Iraq, phone: 009647808271658
Email address: Mmhd@utq.edu.iq

Manal N. Al-Harere,
Department of Applied Sciences, University of Technology, Baghdad, Iraq, phone: 009647703913468
Email address: 100035@uotechnology.edu.iq

Proceedings of International Mathematical Sciences
URL: https://dergipark.org.tr/tr/pub/pims
Volume I Issue 2 (2019), Pages 56-59.

SOLITON SOLUTIONS OF GURSEY MODEL WITH BICHROMATIC FORCE

EREN TOSYALI* AND FATMA AYDOGMUS**

*ISTANBUL BILGI UNIVERSITY, VOCATIONAL SCHOOL OF HEALTH SERVICES

**ISTANBUL UNIVERSITY, DEPARTMENT OF PHYSICS

Abstract. Gursey proposed a spinor field equation which is similar to Heisenberg's nonlinear generalization of Dirac's equation. This equation is the first nonlinear conformal invariant wave equation. In this paper, we investigate the soliton solutions in Gursey wave equation held in a tilted bichromatic force by constructing their Poincaré sections in phase space depending on the system parameters.

1. INTRODUCTION

Gursey proposed a spinor field equation after the successful interpretation of electron and positron by Dirac's nonlinear spinor field wave equation. Gursey Lagrangian is conformal invariant [1]. Gursey had to use a nonpolynomial form to be able to write this Lagrangian. Recently, many studies have been done on Gursey model to understand the quantum properties and dynamics. [2-5]. Also it is known that, solitons are the solutions of nonlinear wave equations and a special kind of localized waves with particle-like behaviours [6]. Soliton type solutions of Gursey model have been found by the use of soler ansatz [7,8]. In this paper, we construct the Poincaré sections of Gursey solitons against bicromatic force may provide us some insight on the subject.

2. MODEL

Gursey spinor wave equation [1] with the positive coupling constant as

$$i\partial\psi = -\frac{4}{3}g(\bar{\psi}\psi)^{\frac{1}{3}} + m\psi \tag{2.1}$$

If we consider the Soler ansatz [7] to find soliton type solutions of Gursey wave equation

2010 *Mathematics Subject Classification.* 35C08, 35Q51, 81R25, 70K05, 70K43.
Key words and phrases. soliton, spinor, nonlinear dynamic.

$$\psi = \begin{bmatrix} g(r)\begin{bmatrix}1\\0\end{bmatrix} \\ if(r)\begin{bmatrix}cos(\theta)\\ e^{i\phi}sin(\theta)\end{bmatrix}\end{bmatrix} e^{-i\omega t} \tag{2.2}$$

Inserting Eq. (2) into Eq. (1), one can obtain

$$i\gamma_\mu \partial_{mu}\psi = \begin{bmatrix} \bar{\omega}g(r) - f'(r) - \frac{2}{r}f(r) \\ 0 \\ -icos(\theta)(\bar{\omega}f(r) + g'(r)) \\ -isin(\theta)e^{i\theta}(\bar{\omega}f(r) + g'(r))\end{bmatrix} e^{-i\omega t} \tag{2.3}$$

and

$$(\bar{\psi}\psi) = g^2(r) - f^2(r) \tag{2.4}$$

with

$$\begin{gathered}\bar{\psi}(\psi^*)^T\gamma^0 = \left[\begin{bmatrix} g(r) \\ 0 \\ -if(r)cos(\theta) \\ -if(r)e^{i\phi}sin(\theta)\end{bmatrix} e^{-i\omega t}\right]^T \\ \bar{\psi} = \begin{bmatrix} g(r) & 0 & -if(r)cos(\theta) & -if(r)e^{-i\phi}sin\theta)\end{bmatrix} e^{i\omega t}\gamma^0 \\ \bar{\psi} = \begin{bmatrix} g(r) & 0 & if(r)cos(\theta) & if(r)e^{-i\phi}sin\theta)\end{bmatrix} e^{i\omega t}\end{gathered} \tag{2.5}$$

Substituting these expressions, the differential equations system can be written as

$$(\bar{\omega} - m)g(r) - f'(r) + \frac{2}{r} + \frac{4}{3}\alpha g(r)(g^2(r) - f^2(r))^{\frac{1}{3}} = 0 \tag{2.6}$$

$$\begin{aligned}-icos(\theta)(\bar{\omega}f(r) + g'(r)) + \frac{4}{3}\alpha(g^2(r) - f^2(r))^{\frac{1}{3}}if(r)cos(\theta) \\ -mf(r)cos(\theta) = 0\end{aligned} \tag{2.7}$$

$$\begin{aligned}-isin(\theta)e^{i\phi}(\bar{\omega}f(r) + g'(r)) + \frac{4}{3}\alpha(g^2(r) - f^2(r))^{\frac{1}{3}}if(r)e^{i\phi}sin(\theta) \\ -mf(r)e^{i\phi}sin(\theta) = 0\end{aligned} \tag{2.8}$$

By the transformations given in Ref. [7] with $r = \frac{\rho}{m+\bar{\omega}}$ and $\nu = \frac{m-\bar{\omega}}{m+\bar{\omega}}$, we achieve the dimensionless form of the nonlinear differential equation system [8] as

$$\frac{dF(\rho)}{d\rho} + \frac{2}{\rho}F(\rho) + \nu G(\rho) - (G^2(\rho) - F^2(\rho))^{\frac{1}{3}}G(\rho) = 0 \tag{2.9}$$

$$\frac{dG(\rho)}{d\rho} + F(\rho) - (G^2(\rho) - F^2(\rho))^{\frac{1}{3}}F(\rho) = 0 \tag{2.10}$$

If we define the externally forced system under the bichromatic force

$$\frac{dF(\rho)}{d\rho} + \frac{2}{\rho}F(\rho) + \nu G(\rho) - (G^2(\rho) - F^2(\rho))^{\frac{1}{3}}G(\rho) = 0 \tag{2.11}$$

$$\frac{dG(\rho)}{d\rho} + F(\rho) - (G^2(\rho) - F^2(\rho))^{\frac{1}{3}} F(\rho) = A_1 cos^2(w_1 H(\rho)) + A_2 cos^2(w_2 H(\rho)) \tag{2.12}$$

$$H(\rho)) = \Omega \tag{2.13}$$

with a $H(\rho)$ function of ρ adding an extra dimension for numerical calculations.

3. NUMERICAL RESULTS

In this paper, we set $m = 1.00007 \times 10^{-9}$, $\bar{\omega} = 9.7 \times 10^{-10}$. Gursey solitons exhibits stable behaviours in phase space without external force as seen in the Figure 1.

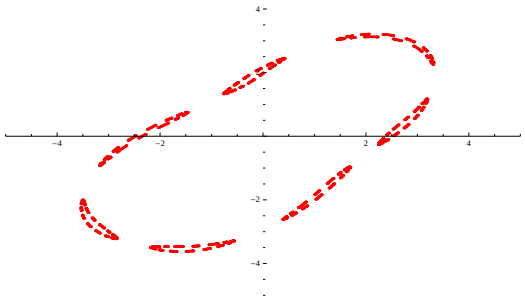

FIGURE 1. Poincaré section diagram without force

In Figure 2, the Poincaré sections are given for $w_1 = 2\pi$, $w_2 = 3\pi$ and the initial conditions are $F(0) = 0.3725$, $G(0) = -0.1652$. The obtained Poincaré sections show the vanishing of the stability of Gursey solitons depending on the parameter values and they exhibit chaotic bahaviours under the bicromatic force.

4. CONCLUSION

In summary, we use the techniques from the viewpoint of nonlinear dynamics in this paper to get more information on spinor type Gursey solitons with bichromatic force. From the obtained numerical results, we can say that the system shows chaotic behaviours depending on the parameter values. As we increase the forcing, the system exhibits more chaotic region. It is known that the study of chaos in soliton physics based on chaos criterion is required interest. We can positively contribute to the work of researchers on this subject as obtaining more results.

5. ACKNOWLEDGMENT

This work was supported by the Scientific Research Projects Coordination Unit of Istanbul University; Project No. FBA-2018-28954

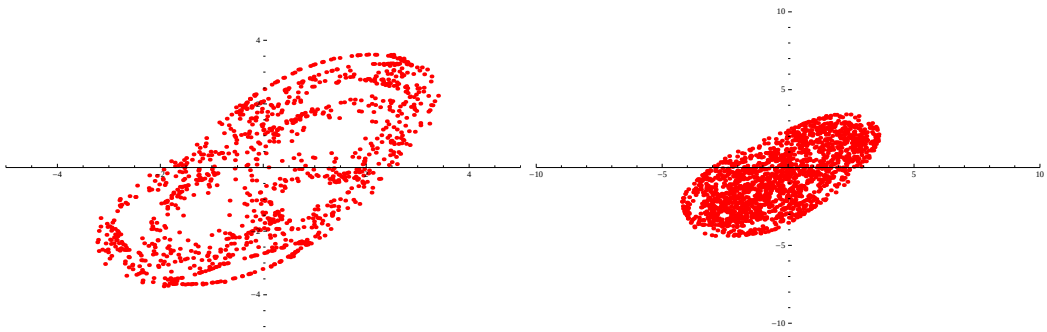

FIGURE 2. Poincaré section diagrams of forcing system for (a) $A_1 = 0.1$, $A_2 = 0.2$ (b) $A_1 = 0.5$, $A_2 = 0.7$

REFERENCES

[1] F. Gursey, On a conform-invariant spinor wave equation, Nuovo Cimento, 1956 3, 988.

[2] F. Aydogmus, Dynamics of Excited Instantons in the System of Forced Gursey Nonlinear Differential Equations, Journal of Experimental and Theoretical Physics, 2015, 120, 2, 210-216.

[3] F. Aydogmus and E. Tosyali, Common Behaviours of Spinor Type Instantons in 2-D Thirring and 4-D Gursey Fermionic Models, Advances in High Energy Physics, 148375 (1-11), (2014).

[4] F. Aydogmus, Chaos in a 4D dissipative nonlinear fermionic model, J. Mod. Phys. C, 2015, 26(7), 1550083.

[5] F. Aydogmus, Unstable Behaviors of Classical Solutions in Spinor-type Conformal Invariant Fermionic Models, Journal of Experimental and Theoretical Physics, 2017, 125, 5, 719-727.

[6] M. Dunajski, Solitons, Instantons, and Twistors, Oxford University Press, New York, 2010.

[7] M. Soler, Ciassical, Stable, Nonlinear Spinor Field with Positive Rest Energy, Phys. Rev. D1, 1970, 2766.

[8] S. Sagaltici, M.S. Thesis, Istanbul University, Institute of Science, Physics Department, Istanbul, Turkey, 2004.

EREN TOSYALI,
ISTANBUL, KUSTEPE, SISLI, TURKEY
Email address: eren.tosyali@bilgi.edu.tr

FATMA AYDOGMUS,
ISTANBUL, VEZNECILER, FATIH, TURKEY
Email address: fatma.aydogmus@cern.ch

Proceedings of International Mathematical Sciences
URL: https://dergipark.org.tr/tr/pub/pims
Volume I Issue 2 (2019), Pages 60-68.

A MATHEMATICAL MODEL OF A ZIKA VIRUS TRANSMISSION WITH IMPACT OF AWARENESS BY MEDIA

PUJI ANDAYANI

UNIVERSITAS INTERNASIONAL SEMEN INDONESIA, PHONE:+6285736033960

Abstract. This paper has studied the transmission of Zika Virus with the impact of media. We analyzed the impact of the awareness programs on social media for the Zika Virus transmission model with saturated incidence rate. The Beddington-De Angelis functional responses used to explain the interaction between a suspected human and an infected human. The dynamical analysis identified by computing the disease-free equilibrium(DFE) and endemic equilibrium(END). The Basic Reproduction Number was identified by Next Generation Matrix(NGM) method. Then the stability of DFE and END were analyzed locally by computing the determinant of Jacobian. The DFE was identified as locally stable when the basic reproduction number was less than unity and was identified as unstable otherwise. Otherwise, the END was identified as existents when the basic reproduction number was greater than unity. The Routh-Hurwitz Criterion showed that the END was locally stable under a specific condition. In the last, the stability of the equilibrium point was also identified numerically depending on certain parameter values.

1. INTRODUCTION

Zika virus is mostly transmitted through a bite from an Aides Aegypti mosquito during the day or night. Zika is also spread through sexual contact between an infected human and an uninfected human. In some cases, Zika is also passed on by pregnant women to her fetus which, causes a birth defect. No vaccine has been found to prevent Zika virus [1]. Based on [2], preventing Zika can be done by using insecticide-treated bed nets and mosquito repellent using a condom and prohibiting pregnant women to travel to the area with Zika outbreak [1].

Recently, most people change their mode of communication from face-to-face into online communication. Social media is one of the best forms of technology that responds to people's needs to communicate and share information online. Some common social media are Facebook, Twitter, Youtube, Whatsapp, and Instagram can be accessed easily by using smartphones and cellular applications [3].

2010 *Mathematics Subject Classification.* Primary: 34D20, 65P40, 37M05.
Key words and phrases. Zika Virus, dynamical analysis, social media, reproduction number, Next Generation Matrix, stability, Routh Hurwitz.

In a disease's epidemiology, social media has an important role to inform the disease's outbreak. Social media and TV advertising is one method to prevent transmission. Misra [4] has made a mathematical model to see the impact of TV advertising and social media on the dynamics of infectious diseases. There are vulnerable populations that are vulnerable to infection as well as populations that often access information through social media. The Zika virus transmission can be informed through social media, then people can take preventive measures. Zika virus outbreak is expected to be controlled or does not spread into outer territory. The mathematical model of social media impact for the epidemiological disease has been researched by some authors. In 2014, the effects of media for influenza epidemic was discussed [5]. The SEIR model was constructed by including the media function. The function $f(I,p)$ was determined to reduce the transmission. In 2018, a mathematical model of Zika virus transmission has been constructed and developed [6] [7]. In this paper, we study the impact of awareness programs on social media. The new parameter m, which becomes the basis of the exponential will be analyzed. We consider some of the trigger factors and preventive actions which are explained in a saturated model using Beddington DeAngelis incident rate.

2. MATHEMATICAL MODEL

A modification model for the Zika virus transmission with the saturated incidence rate and the impact of social media are as follows:

$$\begin{aligned}
\frac{dS_h}{dt} &= \Lambda_h - \frac{\beta_1 e^{mI_h} S_h I_h}{1+\alpha_1 S_h + \alpha_2 I_h} - \frac{\beta_2 S_h I_v}{1+\alpha_3 S_h} - \mu_h S_h, \\
\frac{dI_h}{dt} &= \frac{\beta_1 e^{mI_h} S_h I_h}{1+\alpha_1 S_h + \alpha_2 I_h} + \frac{\beta_2 S_h I_v}{1+\alpha_3 S_h} - (\gamma+\mu_h) I_h, \\
\frac{dR_h}{dt} &= \gamma I_h - \mu_h R_h, \\
\frac{dS_v}{dt} &= \Lambda_v - \beta_3 S_v I_h - \mu_v S_v, \\
\frac{dI_v}{dt} &= \beta_3 S_v I_h - \mu_v I_v,
\end{aligned} \tag{2.1}$$

where $S_h(t), I_h(t), R_h(t), S_v(t), I_v(t)$ stand for suspected human, infected human, recovered human, suspected mosquitoes, and infected mosquitoes respectively. In this study, all of parameters are positive, where Λ_h denote the growth rate of human, Λ_v denote the growth rate of mosquitoes, β_1 is the rate of direct transmission of human, β_2 is the rate of transmission from mosquitoes to human, and β_3 is the rate of transmission from human to mosquitoes. The per capita recovery rate of the infective population defined by $gamma$, α_1, α_2 the parameter that measure the inhibitory effect of human transmission, α_3 the parameter that measure the inhibitory effect of mosquitoes bite, μ_h means the death rate of human, μ_v means the death rate of mosquitoes, respectively.

Let $(S_h, I_h, R_h, S_v, I_v)$ is the solution of the system, with positive initial value. N_h and N_v are the total population of human and mosquitoes respectively, whereas $N_h = S_h + I_h + R_h$ and $N_v = S_v + I_v$. We assume all parameter and variables are

positives. Then the solution of system are in the following :

$$\left\{\Omega = (S_h, I_h, R_h, S_v, I_v) \in {R_+}^5; N_h \leq \frac{\Lambda_h}{\mu_h}, N_v \leq \frac{\Lambda_v}{\mu_v}\right\}. \tag{2.2}$$

The derivation respect to time of the total population of the model 2.1 are :

$$\frac{dN_h}{dt} = \Lambda_h - \mu_h N_h. \tag{2.3}$$

The solution of $\frac{dN_h}{dt} + \mu_h N_h = \Lambda_h$ is $\frac{\Lambda_h}{\mu_h} - Ce^{\mu_h t}$. If $N_h \leq \frac{\Lambda_h}{\mu_h}$, then $\frac{\Lambda_h}{\mu_h} \geq 0$. If $N_h > \frac{\Lambda_h}{\mu_h}$, then $\frac{\Lambda_h}{\mu_h} < 0$. Then choose the initial value as follows :

(1) $N_h(0) = 0$, then the solution is $N_h(t) = \frac{\Lambda_h}{\mu_h}(1 - e^{\mu_h t})$,
(2) $N_h(0) = \frac{\Lambda_h}{\mu_h}$, the solution is $N_h(t) = \frac{\Lambda_h}{\mu_h}$,
(3) $N_h(0) > 0$, the solution is $N_h(t) = \frac{\Lambda_h}{\mu_h}(1 - e^{\mu_h t}) + N_h(0)e^{\mu_h t}$.

The total population of humans and mosquitoes are in the following :

$$0 \leq N_h(t) \leq N_h(t) = \frac{\Lambda_h}{\mu_h}(1 - e^{\mu_h t}) + N_h(0)e^{\mu_h t}, \tag{2.4}$$

and

$$0 \leq N_v(t) \leq N_v(t) = \frac{\Lambda_v}{\mu_v}(1 - e^{\mu_v t}) + N_v(0)e^{\mu_v t}. \tag{2.5}$$

In particular :

$$N_h(t) \leq \frac{\Lambda_h}{\mu_h}, N_v(t) \leq \frac{\Lambda_v}{\mu_v}, \quad \text{when} \quad N_h(0) \leq \frac{\Lambda_h}{\mu_h}, N_v(0) \leq \frac{\Lambda_v}{\mu_v}. \tag{2.6}$$

Then the area $\left\{\Omega = (S_h, I_h, R_h, S_v, I_v) \in {R_+}^5; N_h \leq \frac{\Lambda_h}{\mu_h}, N_v \leq \frac{\Lambda_v}{\mu_v}\right\}$ is bounded.

For $N_h = S_h + I_h + R_h$ and $N_v = S_v + I_v$ then we rewrite the model 2.1 into the following model:

$$\begin{aligned}
\frac{dN_h}{dt} &= \Lambda_h - \mu_h N_h, \\
\frac{dI_h}{dt} &= \left(\frac{\beta_1 e^{mI_h} I_h}{1 + \alpha_1(N_h - I_h - R_h) + \alpha_2 I_h} + \frac{\beta_2 I_v}{1 + \alpha_3(N_h - I_h - R_h)}\right)(N_h - I_h - R_h) - (\gamma + \mu_h)I_h \\
\frac{dR_h}{dt} &= \gamma I_h - \mu_h R_h, \\
\frac{dN_v}{dt} &= \Lambda_v - \mu_v N_v, \\
\frac{dI_v}{dt} &= \beta_3(N_v - I_v)I_h - \mu_v I_v.
\end{aligned} \tag{2.7}$$

3. MATHEMATICAL ANALYSIS

Let the right hand equation of the system 2.7 by zero. Then we found two kinds of equilibrium points, namely disease free equilibrium (DFE) and endemic equilibrium (END) [10]. The disease free equilibrium of the system 2.7 is

$$DFE = ({N_h}^0, {I_h}^0, {R_h}^0, {N_v}^0, {I_v}^0) = \left(\frac{\Lambda_h}{\mu_h}, 0, 0, \frac{\Lambda_v}{\mu_v}, 0\right). \tag{3.1}$$

The DFE is always exists.

Basic reproduction ratio is represent the natural compartmented for disease transmission model, established by the system of ordinary differential equation. In this work, the basic reproduction ration compute by NGM as follows [10].

$$F = \begin{pmatrix} \frac{\beta_1 {N_h}^0}{1+\alpha_1 {N_h}^0} & \frac{\beta_2 {N_h}^0}{1+\alpha_3 {N_h}^0} \\ \beta_3 {N_v}^0 & 0 \end{pmatrix}, \quad V = \begin{pmatrix} \gamma+\mu_h & 0 \\ 0 & \mu_v \end{pmatrix}. \tag{3.2}$$

F is the jacobian of infection matrix with respect to DFE, and V the jacobian matrix which decrease the infection.

$$V^{-1} = \begin{pmatrix} \frac{1}{\gamma+\mu_h} & 0 \\ 0 & \frac{1}{\mu_v} \end{pmatrix}, \quad F.V^{-1} = \begin{pmatrix} \frac{\beta_1 {N_h}^0}{(1+\alpha_1 {N_h}^0)(\gamma+\mu_h)} & \frac{\beta_2 {N_h}^0}{(1+\alpha_3 {N_h}^0)\mu_v} \\ \frac{\beta_3 {N_v}^0}{(\gamma+\mu_h)} & 0 \end{pmatrix}. \tag{3.3}$$

Furthermore, the basic reproduction number is the largest number of eigenvalues of $F.V^{-1}$.

$$R_0 = \frac{R_{01} + \sqrt{R_{01}^2 + 4R_{02}}}{2}; \tag{3.4}$$

where,
$R_{01} = \beta_1 P_1$,
$R_{02} = \beta_2 \beta_3 P_1 P_2 \frac{N_v}{N_h}$.

Lemma 1. *The disease-free equilibrium (DFE) of the system is locally asymptotically stable when $R_0 < 1$ and $N_h < \frac{\mu_v \sigma_2 \delta}{\mu_v \beta_1 \sigma_2 + \beta_2 \beta_3 \sigma_1 N_v}$, otherwise it is unstable.*

Proof. The Jacobian of model 2.7 is

$$J(DFE) = \begin{pmatrix} -\mu_h & -J_0 & 0 & 0 & -J_1 \\ 0 & J_0 - \mu_h - \gamma & 0 & 0 & J_1 \\ 0 & \gamma & -\mu_h & 0 & 0 \\ 0 & -\beta_3 N_v & 0 & -\mu_v & 0 \\ 0 & \beta_3 N_v & 0 & 0 & -\mu_v \end{pmatrix}. \tag{3.5}$$

where,

$J_0 = \frac{\beta_1 N_h}{\sigma_1}$ and $J_1 = \frac{\beta_2 N_h}{\sigma_2}$.
The jacobian of DFE have five eigen values, which are $-\mu_h$, $-\mu_h$ and $-\mu_v$. The two others are analyzed by identify the characteristic polynomials (3.6) as follows,

$$P(\lambda) = \lambda^2 + a_1 \lambda + a_0. \tag{3.6}$$

where,
$a_1 = \frac{1}{\sigma_1}(-\beta_1 N_h + \sigma_1 \delta)$,
$a_0 = \frac{1}{\sigma_1 \sigma_2}(\mu_v \sigma_1 \sigma_2 \delta - N_h(\mu_v \beta_1 \sigma_2 + \beta_2 \beta_3 \sigma_1 N_v))$.

The polynomial 3.6 have two negative real part eigen values, if $a_0 > 0$ which is $N_h < \dfrac{\mu_v \sigma_2 \delta}{\mu_v \beta_1 \sigma_2 + \beta_2 \beta_3 \sigma_1 N_v}$. ■

Lemma 2. *The endemic equilibrium (END) of the system is exist if $R_0 > 1$ and $\alpha_1\delta - (\beta_1 e^{-mI_h} + \alpha_2\mu_h) > 0$.*

Proof. The endemic equilibrium of the system 2.7 is

$$END = (N_h^*, I_h^*, R_h^*, N_v^*, I_v^*). \tag{3.7}$$

Where,
$N_h^* = \dfrac{\Lambda_h}{\mu_h}$, $R_h^* = \dfrac{\gamma}{\mu_h} I_h^*$, $N_v^* = \dfrac{\Lambda_v}{\mu_v}$, and $I_v^* = \dfrac{\beta_3 \Lambda_h}{\mu_v(\beta_3 I_h^* + \mu_v)} I_h^*$.

The poin I_h^* is the positive root of the polynomial $P(I_h^*)$ as follow.

$$P(I_h^*) = b_3 {I_h^*}^3 + b_2 {I_h^*}^2 + b_1 I_h^* + b_0, \tag{3.8}$$

with $\delta = \gamma + \mu_h$, $\Delta = \alpha_1\delta - \alpha_2\mu_h$,
and,
$b_3 = \alpha_3\mu_v\beta_3\delta^2(\alpha_1\delta - (\beta_1 e^{-mI_h^* + \alpha_2}\mu_h))$,
$b_2 = \delta\mu_v[\delta\alpha_3(\mu_v\Delta - (\mu_h\beta_3\varphi_1 + \alpha_2\mu_h)) + \beta_3(\mu_h\varphi_2(\beta_1 e^{-mI_h^*} - \Delta) - \beta_2 N_v\Delta) + \beta_1 e^{-mI_h^*}\alpha_3(\mu_h\beta_3 N_h - \alpha_1\delta)]$,
$b_1 = \mu_h\mu_v[\beta_2\beta_3 N_h N_v\Delta + \mu_v\delta\varphi_2(\beta_1 e^{-mI_h^*} - \Delta) + \mu_h\beta_3\delta\varphi_1\varphi_2 + \delta\varphi_1(\beta_2\beta_3 N_v - \alpha_3\mu_v\delta) + \beta_1 e^{-mI_h^*} N_h\varphi_2(\alpha_3\mu_v\delta - \mu_h\beta_3)]$,
$b_0 = \mu_h^2\mu_v^2(\varphi_1\varphi_2(\delta - N_h\beta_1 e^{-mI_h^*}) - \varphi_1\beta_2\beta_3 N_h\dfrac{N_v}{\mu_v})$.
By calculus, the positiveness of constant b_3, b_2, b_1 and b_0 are identified. Then the polynomial 3.8 have one positive roots if $\alpha_1\delta - (\beta_1 e^{-mI_h + \alpha_2}\mu_h) > 0$. ■

The stability of endemic equilibrium(END) are identified in the following Lemma.

Lemma 3. *The END is locally stable if $(N_v^* - I_v^*) < \dfrac{(\mu_v + \beta_1 I_h^*)(\mu_h K_2 + \gamma K_3)}{\beta_3\mu_h K_4}$.*

Proof. The local stability of END is identified by analyzing the following Jacobian.

$$J(END) = \begin{pmatrix} -\mu_h & 0 & 0 & 0 & 0 \\ K_1 & K_2 & K_3 & 0 & K_4 \\ 0 & \gamma & -\mu_h & 0 & 0 \\ 0 & 0 & 0 & -\mu_v & 0 \\ 0 & -\beta_3(N_v^* - I_v^*) & 0 & \beta_3 I_h^* & -(\beta_3 I_h^* - \mu_v). \end{pmatrix}. \tag{3.9}$$

where,
$K_1 = \Delta_1(\dfrac{1 + \alpha_2 I_h^*}{1 + \alpha_1(N_h^* - I_h^* - R_h^*) + \alpha_2 I_h^*} + \Delta_2\dfrac{1}{1 + \alpha_3(N_h^* - I_h^* - R_h^*)}) > 0$,
$K_2 = -\Delta_1(1 - \dfrac{1 - mI_h^*}{I_h^*}(N_h^* - I_h^* - R_h^*) - \dfrac{(\alpha_2 - \alpha_1)}{1 + \alpha_1(N_h^* - I_h^* - R_h^*) + \alpha_2 I_h^*} - \dfrac{\Delta_2}{1 + \alpha_3(N_h^* - I_h^* - R_h^*)}) -$
$\delta < 0$,
$K_3 = \dfrac{-(1 + \alpha_2 I_h^*)\Delta_1}{1 + \alpha_1(N_h^* - I_h^* - R_h^*) + \alpha_2 I_h^*} - \dfrac{\Delta_2}{1 + \alpha_3(N_h^* - I_h^* - R_h^*)} < 0$,
$K_4 = \dfrac{\beta_2(N_h^* - I_h^* - R_h^*)}{1 + \alpha_3(N_h^* - I_h^* - R_h^*)} > 0$.

Clearly, the eigen value of matrix $J(END)$ are $-\mu_v, -\mu_h$, and the three others are the roots of the following polynomial $P_{END}(\lambda)$.

$$P_{END}(\lambda) = \lambda_3 + c_2\lambda_2 + c_1\lambda_1 + c_0, \tag{3.10}$$

where,
$c_2 = \beta_3 I_h^* + \mu_v + \mu_h - K_2 > 0$,
$c_1 = \mu_v\mu_h - K_2(\mu_v + \mu_h) + \beta_3 I_h^*(\mu_h - K_2) + \beta_3 K_4(I_v^* - N_v^*) - \gamma K_3 > 0$,
$c_0 = -\beta_3\mu_h K_4(N_v^* - I_v^*) - (\mu_v + \beta_3 I_h^*)(\mu_h K_2 + \gamma K_3)$.
By using Routh-Hurwitz Criterion [8] the polynomial $P_{END}(\lambda)$ have three negative real parts eigenvalue since $c_2 > 0$, and $c_1c_2 - c_0 > 0$. Then, the parameter $c_0 > 0$ when $(N_v^* - I_v^*) < \dfrac{(\mu_v\beta_1 I_h^*)(\mu_h K_2 + \gamma K_3)}{\beta_3\mu_h K_4}$. Hence, the the END is locally stable under condition $(N_v^* - I_v^*) < \dfrac{(\mu_v + \beta_1 I_h^*)(\mu_h K_2 + \gamma K_3)}{\beta_3\mu_h K_4}$. ■

4. NUMERICAL RESULT AND DISCUSSION

In this section, we describe the numerical simulation of the model 2.7 to verify the analytical result. Under some certain condition which satisfies the qualification of basic reproduction number, the trajectory of the system 2.7 are identified. The sensitivity analysis also needs to analyze the most sensitive parameter in the model. For simulation, we choose some parameter value which satisfies the qualification condition. The following table provides the parameter description and the parameter value which is used in the numerical simulation.

TABLE 1. The parameter probability by [6] [11]

Parameter	Probability(value)
Λ_h	$\mu_h N_h$ (person per-day)
μ_h	$\frac{1}{\text{lifetime}} = \frac{1}{65x365} = 0.00004215$ (per-day)
α_1	$0 \leq \alpha_1 \leq 1$ (person x day)
β_1	$0 \leq \beta_1 \leq 1$ (person x day)
β_2	$0 \leq \beta_2 \leq 1$ (person x day)
β_3	$0 \leq \beta_3 \leq 1$ (mosquitoes x day)
γ	$0 \leq \gamma \leq 1, \gamma = \frac{1}{recoverytime} = \frac{1}{7} = 0.1428$ (per-day)
Λ_v	$\mu_v N_v$ (mosquitoes per-day)
μ_v	$\frac{1}{\text{lifetime}} = \frac{1}{14} = 0.0714$ (per-day)

Then take the parameter values as follow : $\Lambda_h = 0.004215, \mu_h = 0.00004215, \mu_v = 0.0714, \beta_1 = 0.0001, \beta_2 = 0.002, \beta_3 = 0.0001, \gamma = 0.1428, \Lambda_v = 71.4, m = 2, \alpha_1 = 0.95, \alpha_2 = 0.1$, and $\alpha_3 = 0.96$. Under that parameter value than we have the following result.

The figure 1a and figure 1b tell us the trajectories of the system 2.7 when the basic reproduction number is less than unity. The solution of the system will tends to the suspect human and mosquitoes which means the infected population is extinct. Then the system is free from disease along certain times.

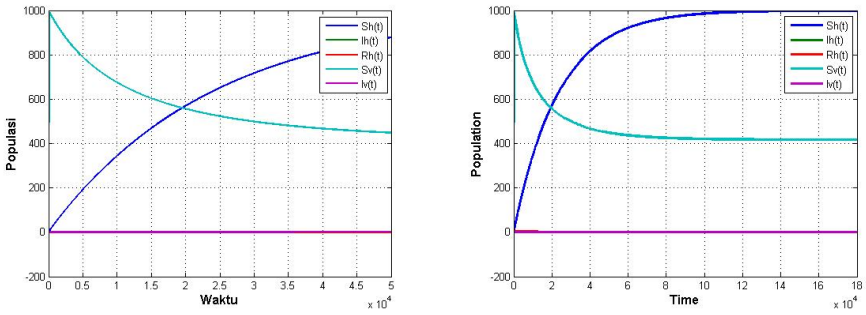

(A) Simulation 1 (B) Simulation 2

FIGURE 1. Numerical Result of model (2.7) when $R_0 < 1$, (a) Simulation when $t = 4000$ (b) Simulation when $t = 18000$

The sensitivity analysis was performed to determine the relative importance of model parameters of disease transmission. Choose the parameter value, $\mu_v = 0.0714, \mu_h = 0.00004215, \Lambda_h = 10, \Lambda_v = 20, \beta_1 = 0.02, \beta_2 = 0.0007, \beta 3 = 0.01, \alpha_1 = 0.35, \alpha_3 = 0.95, \gamma = 0.1428$. Based on mathematical computation and normalization the sensitivity index of R_0, we have the following result (Table 1).

TABLE 2. Table of sensitivity index for each parameter of the system 2.7

Parameter	Sensitivity Index	Interpretation (Increasing or decreasing)	Rank
Λ_h	0.00000621	Λ_h by 10%, R_0 increasing by 0.000621%	7
μ_h	-0.000213693	μ_h by 10%, R_0 decreasing by 0.021%	6
α_1	-0.40627261	α_1 by 10%, R_0 decreasing by 40.6%	4
α_2	0	α_2 by 10%, R_0 by increasing 0%	8
α_3	-0.296859936	α_3 by 10%, R_0 decreasing by 29.6%	3
β_1	0.4062775	β_1 by 10%, R_0 increasing by 40.6%	4
β_2	0.296861253	β_2 by 10%, R_0 increasing by 29.6%	5
β_3	0.296861253	β_3 by 10%, R_0 increasing by 29.6%	5
γ	-0.7029312644	γ by 10%, R_0 decreasing by 70.2%	1
Λ_v	0.4975303648	Λ_v by 10%, R_0 increasing by 49%	3
μ_v	-0.5937225055	μ_v by 10%, R_0 decreasing by 59.3%	2

According to table 2, we can see that the most sensitive parameter of the model x is the recovery rate of the infection population (γ). The second one is the death rate of mosquitoes (μ_v) and the third one is the parameter that measures the inhibitory effect of mosquitoes bite (α_3). The solution we can do to prohibit the problem of Zika virus, beginning with the pursuit of healing of infected humans, such as conducting treatment and providing vaccines. Then reduce the mosquito population by maintaining environmental cleanliness and prevent mosquito-spread according to government recommendations. Additionally, by taking precautions to be free from Aedes Aegyepti mosquito bites. Conversely, the least sensitive parameter is the parameter that measures the inhibitory effect of human transmission (α_2). So

for further model development, these parameters α_2 do not need to be used.

5. CONCLUSION

In this paper, we have discussed the interaction among human which suspected, infected, recovered from Zika virus and mosquitoes which infected and suspected Zika. The parameter of social media is also used to see the impact on that model. To see the effects of social media on the transmission of Zika virus, mathematical models using systems with five nonlinear differential equations were constructed. The boundedness problem of the system is analyzed and proved by ordinary mathematical calculations. By letting the right-hand side of the system by zero, the two types of equilibrium points were obtained with a certain existing condition, namely disease-free and endemic. The basic reproduction numbers are the basis for the conditions of stability and the existence of equilibrium points, were found by using the Next Generation Matrix (NGM). The dynamical analysis has been solved out by using supporting theorems such as Descartes and Routh-Hurwitz criteria. Based on the analytical result, the disease-free equilibrium points are locally asymptotically stable when the basic reproduction number was less than unity. Moreover, the endemic equilibrium point exists and locally stable when the basic reproduction number is more than unity and satisfied the certain parameter requirement. The sensitivity analysis is also analyzed to identify the sensitivity of each parameter of the model. Then, the most sensitive parameter of the model 2.7 is the recovery rate of the infective population (γ). Conversely, the least sensitive parameter is the inhibitory effect of human transmission (α_2). It becomes a recommendation for the next model development, the parameters α_2 is no need to be used. Numerical simulations of the dynamic behavior of equilibrium points were also presented to complete the analytical results. Then generally it can be concluded that social media affect reducing the spread of the Zika virus.

6. ACKNOWLEDGEMENT

The authors give deep gratitude to Direktorat Riset dan Pengabdian Masyarakat (DRPM), Direktorat Jenderal Penguatan Riset dan Pengembangan, the Ministry of Research, Technology, and Higher Education, Indonesia for the funding support. The author also expresses big thanks to Research and Human Responsibility Institute of Universitas International Semen Indonesia and the crew of the Informatics department, for the greatest support.

References

[1] U.S. Department of Health and Human Services. Zika Transmission. Comput. "(from Center for Disease Control and Prevention: https://www.cdc.gov/zika/transmission/index.html).
[2] P. Padmanabhan, P.Seshaiyer, and C.Castillo-Chavez. *Letters in Biomathematics.* **4** (2017) 148–166.
[3] A. Ishaku, B.S.Musa, A.Sanda, and A.M.Bakoji,*IOSR Journal of Mathematics.* **4** (2018) 72–79.
[4] A. Ishaku, B.S.Musa, A.Sanda, and A.M.Bakoji,*Mathematical Biosciennces and Engineering.* **15** (2018) 72–79.
[5] S. Collinson and J.M.Heffernan,*BMC Public Health.* **4** (2014) 1–10.
[6] P. Andayani, L.R.Sari, A.Suryanto, and I.Darti,*Far East Journal of Mathematical Sciences(FJMS).* **11** (2019) 145–157.
[7] P. Andayani, L.R.Sari, A.Suryanto, and I.Darti,*J. Exp. Life Sci..* **8** (2019) 161–164.

[8] Yang, X.,*Applied Mathematics Letters*. **15** (2002) 615–621.
[9] Kemp, Simon,DIGITAL 2019: Global Digital Overview. https://datareportal.com/reports/digital-2019-global-digital-overvie.
[10] Andayani, Puji. The Effect of Social Media for a Zika Virus Transmission with Beddington De Angelis Incidence Rate: Modeling and Analysis. *AIP Conference Proceedings*. **2183** (2019) 1–5.
[11] Andayani, Puji. *Jurnal Matematika dan Sains*. **24** (2019) 19–23.

Kompleks PT. Semen Indonesia, Jl. Veteran,
Gresik City, Indonesia, Phone:+6285736033960
Email address: puji.andayani@uisi.ac.id

Proceedings of International Mathematical Sciences
URL: https://dergipark.org.tr/tr/pub/pims
Volume I Issue 2 (2019), Pages 69-76.

THE EXPLICIT RELATION BETWEEN THE DKP EQUATION AND THE KLEIN-GORDON EQUATION

DJAHIDA BOUCHEFRA*, AND BADREDINE BOUDJEDAA**

*DEPARTMENT OF MATHEMATICS AND COMPUTER SCIENCE, INSTITUTE OF SCIENCES AND TECHNOLOGY, UNIVERSITY CENTER ABDELHAFID BOUSSOUF-MILA, 43000 MILA, ALGERIA.

LABORATORY OF MATHEMATICS AND THEIR INTERACTIONS (MELILAB).
D.BOUCHEFRA@CENTRE-UNIV-MILA.DZ.

**DEPARTMENT OF MATHEMATICS AND COMPUTER SCIENCE, INSTITUTE OF SCIENCES AND TECHNOLOGY, UNIVERSITY CENTER ABDELHAFID BOUSSOUF-MILA, 43000 MILA, ALGERIA.

Abstract. DKP equation describes spin-0 and spin-1 relativistic particles. Many researchers have been interested in the DKP equation. In this work, we give an explicit relation between the DKP and the KG equations for both the spin-0 particle in $(1+3)$ dimensions and spin-1 particle in $(1+1)$ dimensions. From the DKP equation in its explicit form, we get another system generated by the KG equation, which gives us the equivalence between the DKP equation and the KG equation. Using this equivalence, the Volkov-like solution of the DKP equation for the spin-0 particle in the field of an electromagnetic plane wave, is calculated.

1. Introduction

Relativistic quantum mechanics is the branch of quantum mechanics that deals with the motion of relativistic particles. Among the most known equations in the relativistic quantum mechanics are: the Klein-Gordon equation (KG equation), which describes spinless particles, i.e. the spin-0 particles (e.g. the Higgs boson ...), the Dirac equation, which describes the spin-$\frac{1}{2}$ particles (e.g. electron, positron and neutrinos ...) and the Proca equation, which describes the spin-1 particles (e.g. the photon ...). Petiau [1], Duffin [2] and Kemmer [3] were motivated by Dirac's work for the spin-$\frac{1}{2}$ relativistic particle; they gave an equation (DKP equation) that describes spin-0 and spin-1 relativistic particles, which is an equation similar to the Dirac equation and in which the gamma matrices (γ) are replaced by the beta matrices (β), where the (β) matrices are 5×5 matrices for the spin-0 particle

2010 *Mathematics Subject Classification.* 35Q40 ; 35Q60 ; 35Q70 ; 70G70 ; 81T10 ; 83C50.
Key words and phrases. Equation of Duffin-Kemmer-Petiau; Algebra DKP; Klein-Gordon equation; Volkov solution.

and 10×10 matrices for the spin-1 particle, which satisfies a different algebra from the algebra of the (γ) matrices for the Dirac equation.

In recent decades, many researchers have been interested in the DKP equation. Fischbach et al. [4], Krajcik et al. [5] have been interested in the equivalence of the DKP equation with the KG and the Proca equations. Nedjadi et al. [6] have studied some properties of the DKP equation and have also addressed the unresolved problem of the spinless DKP boson in a central field. Fainberg et al. [7] provided an equivalence between DKP and KG theories. They established this equivalence via the matrix S and the reduction formula LSZ (Lehmann-Symanzik-Zimmermann). They used the in and out asymptotic solutions and different diagrams generated by the generating function. Lunardi et al. [8] have discussed two problems relative to the electromagnetic coupling of DKP theory: the presence of an anomalous term in the Hamiltonian form of the theory and the apparent difference between the interaction terms in DKP and KG Lagrangians. Chetouani et al. [9] have solved the DKP equation in the presence of step potential. Merad [10] solved the DKP equation for spin-0 and spin-1 with smooth potential and position dependent-mass where the solution is given in terms of the Heun function. Boutabia-Chéraitia et al. [11] presented a calculation of the Green's function of the DKP equation in the case of scalar and vectorial particles interacting with a square barrier potential and its relation to the KG equation. Recently, Lunardi [12] has shown that the supposed spin-1 sector of the theory restricted to $(1+1)$ space-time dimensions actually is unitarily equivalent to its spin-0 sectors.

This work is organized as follows: In Section 2, we give the DKP equation for the spin-0 with 5×5 beta matrices and 10×10 beta matrices for the spin-1. In Section 3, we give an explicit relation, which is a direct equivalence, between the DKP and the KG equations for the spin-0 particle in $(1+3)$ dimensions and for the spin-1 particle in $(1+1)$ dimensions. The equivalence for the spin-0 particle is established not only in the free case but even in the presence of any interaction. In Section 4, using this relation, we calculate the Volkov-like solution of the DKP equation for the spin-0 particle, i.e. in the same form as the Volkov solution of the KG equation [13], in the field of an electromagnetic plane wave.

This paper is the full length paper of the AIP extended abstract [14].

2. The DKP equation

The DKP equation (for $\hbar = 1$, $c = 1$) interacting with an electromagnetic field A_μ is given by

$$[i\beta^\mu(\partial_\mu + ieA_\mu) - m]\psi = 0^{[1]}, \tag{2.1}$$

where m is the particle's mass and β^μ are square matrices satisfying the following algebra

$$\beta^\mu\beta^\nu\beta^\lambda + \beta^\lambda\beta^\nu\beta^\mu = g^{\mu\nu}\beta^\lambda + g^{\nu\lambda}\beta^\mu, \tag{2.2}$$

[1]We use the following notations $\partial_\mu = (\partial_0, \nabla)$, $A_\mu = (A_0, -\mathbf{A})$ with the convention $\sum_\mu a^\mu b_\mu = a^\mu b_\mu$.

$g^{\mu\nu}$ is the metric tensor of Minkowski as $g^{\mu\nu} = \mathrm{diag}\,(1,-1,-1,-1)$. The β^μ are 5×5 matrices for the spin-0 particle and 10×10 matrices for the spin-1 particle.

For the spin-0, the β^μ matrices are given by

$$\beta^0 = \begin{pmatrix} \theta & \bar{0} \\ \bar{0}^T & \mathbf{0} \end{pmatrix}, \quad \beta^i = \begin{pmatrix} \tilde{0} & \rho_i \\ -\rho_i^T & \mathbf{0} \end{pmatrix}, \quad i = 1,2,3 \tag{2.3}$$

where

$$\theta = \begin{pmatrix} 0 & 1 \\ 1 & 0 \end{pmatrix}, \quad \rho_1 = \begin{pmatrix} -1 & 0 & 0 \\ 0 & 0 & 0 \end{pmatrix}, \tag{2.4}$$

$$\rho_2 = \begin{pmatrix} 0 & -1 & 0 \\ 0 & 0 & 0 \end{pmatrix}, \quad \rho_3 = \begin{pmatrix} 0 & 0 & -1 \\ 0 & 0 & 0 \end{pmatrix}. \tag{2.5}$$

$\bar{0}, \tilde{0}$ and $\mathbf{0}$ are 2×3, 2×2 and 3×3 zero matrices, respectively, and ρ^T denotes the transpose of matrix ρ.

For the spin-1, the β^μ matrices are given by

$$\beta^0 = \begin{pmatrix} 0 & \bar{0} & \bar{0} & \bar{0} \\ \bar{0}^T & \mathbf{0} & \mathbf{1} & \mathbf{0} \\ \bar{0}^T & \mathbf{1} & \mathbf{0} & \mathbf{0} \\ \bar{0}^T & \mathbf{0} & \mathbf{0} & \mathbf{0} \end{pmatrix}, \quad \beta^i = \begin{pmatrix} 0 & \bar{0} & e_i & \bar{0} \\ \bar{0}^T & \mathbf{0} & \mathbf{0} & -is_i \\ -e_i^T & \mathbf{0} & \mathbf{0} & \mathbf{0} \\ \bar{0}^T & -is_i & \mathbf{0} & \mathbf{0} \end{pmatrix}, \quad i = 1,2,3 \tag{2.6}$$

where e_i and $\bar{0}$ are given by

$$e_1 = (1,0,0), \quad e_2 = (0,1,0), \quad e_3 = (0,0,1), \quad \bar{0} = (0,0,0). \tag{2.7}$$

$\mathbf{1}$ denoting the 3×3 unity matrix. The s_i being the standard non-relativistic 3×3 spin-1 matrices

$$s_1 = \begin{pmatrix} 0 & 0 & 0 \\ 0 & 0 & -i \\ 0 & i & 0 \end{pmatrix}, s_2 = \begin{pmatrix} 0 & 0 & i \\ 0 & 0 & 0 \\ -i & 0 & 0 \end{pmatrix}, s_3 = \begin{pmatrix} 0 & -i & 0 \\ i & 0 & 0 \\ 0 & 0 & 0 \end{pmatrix}. \tag{2.8}$$

3. The explicit relation between the DKP equation and the KG equation

3.1. **Spin-0 particle.** As described above, the DKP equation for the spin-0 particle in $(1+3)$ dimensions is given by equation (2.1) where the β^μ are 5×5 matrices given by the relation (2.3).

For $\psi=(\psi_1,\psi_2,\psi_3,\psi_4,\psi_5)^T$, which is a solution of the equation (2.1). Then the equation (2.1) can be written in its compact form as

$$(I)\begin{cases} iD^\mu\psi_{\mu+2}-m\psi_1=0, & (3.1)\\ iD_\mu\psi_1-m\psi_{\mu+2}=0, \qquad \mu=0,1,2,3, & (3.2)\end{cases}$$

where $D_\mu=(\partial_\mu+ieA_\mu)$.

From the equations (3.2), it's easy to see that each component ψ_2,ψ_3,ψ_4 and ψ_5 depends on ψ_1 as

$$(II)\qquad \psi_{\mu+2}=\frac{i}{m}D_\mu\psi_1, \qquad \mu=0,1,2,3.$$

Replacing each component ψ_2,ψ_3,ψ_4 and ψ_5 of the system (II) in the equation (3.1), of the system (I), we obtain

$$(D^\mu D_\mu+m^2)\psi_1=0, \tag{3.3}$$

which is KG equation for ψ_1.

In other words, the DKP equation (2.1) (i.e. system (I)) and the KG equation (3.3), for the spin-0 particle, are equivalent in the sense that if ψ_1 is a solution of the KG equation (3.3) , the solution of the DKP equation (2.1) is given by ψ where ψ_2,ψ_3,ψ_4 and ψ_5 are given by the system (II), and conversely, if ψ is a solution of the DKP equation (2.1) (i.e. solution of the system (I)), then ψ_1 is the solution of the KG equation (3.3).

Remark. *This equivalence, i.e. the relation between the DKP equation and the KG equation is established in the same manner for both* $(1+2)$ *dimensions and* $(1+1)$ *dimensions.*

3.2. **Spin-1 particle.** In the same way, as in the previous part, we can find an explicit relation between the DKP equation and the KG equation for the spin-1 particle in $(1+1)$ dimensions. The DKP equation for the spin-1 particle in $(1+1)$ dimensions is given by

$$[i\beta^0(\partial_0+ieA_0)+i\beta^1(\partial_1-ieA_1)-m]\psi=0, \tag{3.4}$$

where the β^0 and β^1 are 10×10 matrices given by the relation (2.6). Then if ψ is written as

$$\psi=(\psi_1,\psi_2,\psi_3,\psi_4,\psi_5,\psi_6,\psi_7,\psi_8,\psi_9,\psi_{10})^T, \tag{3.5}$$

the equation (3.4), written in its explicit form, takes the following form

$$(III)\begin{cases}(i\partial_1+eA_1)\psi_5-m\psi_1=0, & (3.6)\\ (i\partial_0-eA_0)\psi_5-m\psi_2=0, & (3.7)\\ (i\partial_0-eA_0)\psi_6-(i\partial_1+eA_1)\psi_{10}-m\psi_3=0, & (3.8)\\ (i\partial_0-eA_0)\psi_7+(i\partial_1+eA_1)\psi_9-m\psi_4=0, & (3.9)\\ (i\partial_0-eA_0)\psi_2-(i\partial_1+eA_1)\psi_1-m\psi_5=0, & (3.10)\\ (i\partial_0-eA_0)\psi_3-m\psi_6=0, & (3.11)\\ (i\partial_0-eA_0)\psi_4-m\psi_7=0, & (3.12)\\ -m\psi_8=0, & (3.13)\\ -(i\partial_1+eA_1)\psi_4-m\psi_9=0, & (3.14)\\ (i\partial_1+eA_1)\psi_3-m\psi_{10}=0. & (3.15)\end{cases}$$

From equations (3.6), (3.7), (3.11), (3.12), (3.13), (3.14) and (3.15), we can easily see that each component depends on ψ_3, ψ_4 and ψ_5, and we get the following system

$$(IV)\begin{cases}\psi_1=\dfrac{1}{m}(i\partial_1+eA_1)\psi_5, & (3.16)\\ \psi_2=\dfrac{1}{m}(i\partial_0-eA_0)\psi_5, & (3.17)\\ \psi_6=\dfrac{1}{m}(i\partial_0-eA_0)\psi_3, & (3.18)\\ \psi_7=\dfrac{1}{m}(i\partial_0-eA_0)\psi_4, & (3.19)\\ \psi_8=0, & (3.20)\\ \psi_9=\dfrac{-1}{m}(i\partial_1+eA_1)\psi_4, & (3.21)\\ \psi_{10}=\dfrac{1}{m}(i\partial_1+eA_1)\psi_3. & (3.22)\end{cases}$$

If we replace each component $\psi_1, \psi_2, \psi_6, \psi_7, \psi_9$ and ψ_{10} of the system (IV) in equations (3.8), (3.9) and (3.10) we get

$$(V)\begin{cases}(D^\mu D_\mu+m^2)\psi_3=0, & (3.23)\\ (D^\mu D_\mu+m^2)\psi_4=0, \qquad (\mu=0,1) & (3.24)\\ (D^\mu D_\mu+m^2)\psi_5=0. & (3.25)\end{cases}$$

Equations (3.23), (3.24) and (3.25) are the KG equations interacting with an electromagnetic field A_μ for each component ψ_3, ψ_4 and ψ_5 respectively.

More precisely, the DKP equation (3.4) and the KG equations (3.23), (3.24) and (3.25) for ψ_3, ψ_4 and ψ_5 respectively are equivalent. Indeed, if ψ_3, ψ_4 and ψ_5 are solutions of the KG equations (i.e. system (V)) so ψ is a solution of the system (III) i.e. DKP equation (3.4), where $\psi_1, \psi_2, \psi_6, \psi_7, \psi_8, \psi_9$ and ψ_{10} are given by the system (IV), and conversely, if ψ is the solution of the DKP equation (3.4), ψ_3, ψ_4 and ψ_5 are solutions of the KG equations in the system (V).

Remark. *This equivalence, i.e. the relation between DKP equation and KG equation for the spin-1 particle in* $(1+1)$ *dimensions, can be established in the same way if we use* β^2 *or* β^3 *instead of* β^1.

4. Application

4.1. **Volkov-like solution for the spin-0 particle.** Now, we are interested in using this equivalence between the DKP equation and the KG equation (i.e. equivalence between system (I) and equation (3.3)) to calculate the Volkov-like solution of the DKP equation (2.1) for the spin-0 particle in the field of an electromagnetic plane wave.

So if the solution of the DKP equation (2.1) is

$$\psi = (\psi_1, \psi_2, \psi_3, \psi_4, \psi_5)^T, \tag{4.1}$$

then by this equivalence, ψ_1 is the solution of the KG equation (3.3), ψ_2, ψ_3, ψ_4 and ψ_5 are given by the system (II).

We know that the Volkov solution ψ_1, solution of KG equation (3.3), in the field of an electromagnetic plane wave is given by

$$\psi_1 = Ce^{-ipx}F_1(\phi), \quad \text{for } \phi = kx, \tag{4.2}$$

where C is a normalisation constant, and F_1 is a solution of the differential equation

$$2i(kp)F_1'(\phi) + [-2e(pA) + e^2A^2]F_1(\phi) = 0, \tag{4.3}$$

then, we find

$$F_1'(\phi) = -i\left[\frac{e}{(kp)}(pA) - \frac{e^2}{2(kp)}A^2\right]F_1(\phi), \tag{4.4}$$

i.e.

$$F_1(\phi) = \exp\left(-i\int_0^{kx}\left[\frac{e}{(kp)}(pA) - \frac{e^2}{2(kp)}A^2\right]d\phi\right). \tag{4.5}$$

Then from the system (II), $\psi = (\psi_1, \psi_2, \psi_3, \psi_4, \psi_5)^T$ is a Volkov-like solution of the DKP equation (2.1) for the spin-0 particle in the field of an electromagnetic plane wave, i.e.

$$(VI)\begin{cases} \psi_1 = C\exp\{-iS\}, & (4.6)\\ \psi_{\mu+2} = \dfrac{1}{m}\left[k_\mu\left(\dfrac{e}{(kp)}(pA) - \dfrac{e^2}{2(kp)}A^2\right) + p_\mu - eA_\mu\right]\psi_1, \quad \mu = 0,1,2,3, & (4.7)\end{cases}$$

where $S = px + \int_0^{kx}\left[\frac{e}{(kp)}(pA) - \frac{e^2}{2(kp)}A^2\right]d\phi$, is the classical action of the system.

5. Conclusion

In relativistic quantum mechanics, the DKP equation occupies an important place in the description of the spin-0 and the spin-1 particles. The DKP equation is a very interesting equation in relativistic quantum mechanics. In the last decades, the DKP equation has attracted the attention of many researchers and has been studied in its various aspects.

In this paper, we discussed two points relating to the explicit relation between the DKP equation and the KG equation for the description of particles, one for the spin-0 particles in $(1+3)$ dimensions and the other for the spin-1 particles in $(1+1)$ dimensions. The results of this work are important and interesting, where we have shown that the equivalence of these equations is established for any wave function, not only in the free case, but even in the presence of any interaction for both the spin-0 particle in $(1 + 3)$ dimensions and spin-1 particle in $(1 + 1)$ dimensions. Moreover, we found a Volkov-like solution to the DKP equation for spin-0 particles in the presence of an electromagnetic field.

Acknowledgments. The authors would like to thank the anonymous reviewers for their remarks and suggestions that helped us to improve the writing of this work. Thanks to Professor T. Boudjedaa for his fruitful and helpful advice in elaborating this work.

References

[1] G. Petiau, Contribution à la théorie des équations d'ondes corpusculaires, Ph.D. thesis, University of Paris, 1936. Published in Acad. Roy. de Belg., Classe Sci., Mem in 8° **16**(2) (1936).
[2] R.J. Duffin, On the characteristic matrices of covariant systems, Phys. Rev. **54** (1938) 1114.
[3] N. Kemmer, The particle aspect of meson theory, Proc. R. Soc. A **173**(952) (1939) 91-116.
[4] E. Fischbach, M.M. Nieto, and C.K. Scott, The Association of the Sakata-Taketani (Feshbach-Villars) Field with the Kemmer Field, under Symmetry Breaking, Prog. Theor. Phys. **48**(2) (1972) 574-595.
[5] R.A. Krajcik, and M.M. Nieto, Bhabha first-order wave equations: I. C, P, and T, Phys. Rev. D **10**(12) (1974) 4049-4063.
[6] Y. Nedjadi, and R.C. Barrett, On the properties of the Duffin-Kemmer-Petiau equation, J. Phys. G: Nucl. Part. Phys. **19** (1993) 87-98.
[7] V.Ya. Fainberg, and B.M. Pimentel, On equivalence of Duffin-Kemmer-Petiau and Klein-Gordon equations, B. J. Phys. **30**(2) (2000) 275-281.
[8] J.T. Lunardi, B.M. Pimentel, R.G. Teixeira, and J.S. Valverde, Remarks on Duffin-Kemmer-Petiau theory and gauge invariance, Phys. Lett. A **268**(3) (2000) 165-173.
[9] L. Chetouani, M. Merad, T. Boudjedaa, and A. Lecheheb, Solution of Duffin-Kemmer-Petiau equation for the step potential, Int. J. Theor. Phys. **43**(4) (2004) 1147-1159.
[10] M. Merad, DKP equation with smooth potential and position-dependent mass, Int. J. Theor. Phys. **46**(8) (2007) 2105-2118.
[11] B. Boutabia-Chéraitia, and T. Boudjedaa, The Green function for the Duffin-Kemmer-Petiau equation, J. Geom. Phys. **62**(10) (2012) 2038-2043.
[12] J.T. Lunardi, A note on the Duffin-Kemmer-Petiau equation in $(1 + 1)$ space-time dimensions, J. Math. Phys. **58** (2017) 123501.
[13] V.B. Berestetskii, E.M. Lifshitz, and L.P. Pitaevskii, Quantum electrodynamics, Pergamon Press Ltd., Headingt.on Hill Hall, Oxford OX3 OBW, England. Vol **4**. 2nd ed (1982).
[14] D. Bouchefra, and B. Boudjedaa, The explicit relation between the DKP equation and the Klein-Gordon equation, to appear in AIP Conference Proceedings of Third International Conference of Mathematical Sciences (ICMS 2019).

Djahida Bouchefra,
Department of Mathematics and Computer Science, Institute of Sciences and Technology, University Center Abdelhafid Boussouf- Mila, 43000 Mila, Algeria.
Laboratory of Mathematics and their interactions (Melilab).
Email address: d.bouchefra@centre-univ-mila.dz

Badredine Boudjedaa,
Department of Mathematics and Computer Science, Institute of Sciences and Technology, University Center Abdelhafid Boussouf- Mila, 43000 Mila, Algeria.
Email address: b.boudjedaa@centre-univ-mila.dz -- badredineb@gmail.com